

# An efficient numerical method based on exponential B-splines for time-fractional Black-Scholes equation governing European options

Anshima Singh<sup>a</sup>, Sunil Kumar<sup>a</sup>

<sup>a</sup>*Department of Mathematical Sciences, Indian Institute of Technology (BHU) Varanasi, Uttar Pradesh, India*

---

## Abstract

In this paper a time-fractional Black-Scholes model (TFBSM) is considered to study the price change of the underlying fractal transmission system. We develop and analyze a numerical method to solve the TFBSM governing European options. The numerical method combines the exponential B-spline collocation to discretize in space and a finite difference method to discretize in time. The method is shown to be unconditionally stable using von-Neumann analysis. Also, the method is proved to be convergent of order two in space and  $2 - \mu$  in time, where  $\mu$  is order of the fractional derivative. We implement the method on various numerical examples in order to illustrate the accuracy of the method, and validation of the theoretical findings. In addition, as an application, the method is used to price several different European options such as the European call option, European put option, and European double barrier knock-out call option.

*Key words:* Time-fractional, Black-Scholes model, European option, Exponential B-splines, Collocation method.

---

## 1. Introduction

In the market of finance, investors need to minimize and control risks. By market risks, we mean the chances of the deficit because of those aspects that impact the inclusive performance of the markets. Investors can manage these types of risks by investing in significant instruments that remove the risk of price volatility. Such instruments are known as financial derivatives. The value of a financial derivative depends on the functioning of the underlying asset. Among many financial derivatives, an option is one of the most well-known and important derivatives, so pricing an option is a significant problem both in practice and in theory. In 1973, Black and Scholes [1] and Merton [2] had proposed the Black-Scholes model, which gives an accurate delineation of the behavior of the underlying asset. Black-Scholes model is a second-order parabolic partial differential equation with respect to stock price and time, that governs the European option value on a stock,

---

*Email addresses:* anshima.singh.rs.mat18@iitbhu.ac.in (Anshima Singh)

whose price pursues the geometric Brownian motion with fixed interest rate and constant volatility. Since the Black-Scholes model is simple and effective to model option value, it led to a revolution in the financial market over the past several decades. The classical Black-Scholes model is given by [3, 4]

$$\frac{\partial \mathcal{V}(\xi, \tau)}{\partial \tau} + \frac{\sigma^2 \xi^2}{2} \frac{\partial^2 \mathcal{V}(\xi, \tau)}{\partial \xi^2} + (r_f - D_Y) \xi \frac{\partial \mathcal{V}(\xi, \tau)}{\partial \xi} - r_f \mathcal{V}(\xi, \tau) = 0, \quad (\xi, \tau) \in \mathbb{R}^+ \times (0, \tilde{T}), \quad (1)$$

with the terminal condition

$$V(\xi, \tilde{T}) = \max(\xi_{\tilde{T}} - \tilde{K}, 0), \quad \xi_{\tilde{T}} \geq 0, \quad (2)$$

where  $\mathcal{V}(\xi, \tau)$  denotes the value of a European option price. Here,  $\sigma(\xi, \tau)$ ,  $r_f(\tau)$ ,  $D_Y(\tau)$ ,  $\tilde{T}$ ,  $\tilde{K}$ , and  $\tau$  represent the volatility of the returns from the holding stock price  $\xi$ , the risk free rate, the dividend yield, the expiry time, the exercise price, and the current time respectively. Several approaches have been proposed in the literature to obtain a solution to the classical Black-Scholes model [4–9]. Due to the unrealistic assumptions used in the Black-Scholes model, it has some drawbacks, so it cannot explain a few existing phenomena such as stock price volatility, a short time boom in the financial market. [10], etc.

Fractional integrals and fractional derivatives are non-local, so they are a useful tool to describe memory. Fractional differential equations have become a powerful tool for studying fractal dynamics and fractal geometry. The fractional calculus has had a massive impact on financial theory, as the fractional Black Scholes model can deal with most of the shortcomings of the classical Black Scholes model. Wyss was the first researcher to introduce the time-fractional Black Scholes model for pricing a European call option [11]. To deal with the problem of short time jumps in the financial market, Cartea and del-Castillo-Negrete [12] developed the space fractional Black-Scholes model to price exotic options. Jumarie [13, 14] applied Itô's lemma and the fractional-order Taylor's series method to obtain the time-space fractional Black-Scholes model. He studied the dynamics of the stock exchange and also considered Merton's optimal portfolio to provide new results. Liang et al. [15] derived a bi-fractional Black-Merton-Scholes model. With growth of applications of fractional models in financial field, researchers have shown interest in solving them analytically [16–20] and numerically [21–29].

Spline functions are prevalent in mathematics, computer science, engineering, etc. [30–33]. The use of piecewise cubic polynomial spline interpolation often gives undesirable inflexion points. The exponential spline interpolation method is a generalization of cubic splines and avoids these inflexion points. Pruess [34, 35] showed that exponential splines can generate co-monotone and co-convex interpolants and provided the remedy to the inflexion points issue. Pruess [34], Boorm[36], and McCartin [37] studied the exponential splines in detail. McCartin also showed that the exponential splines accept a basis of B-splines. They are used in approximating the solutions of various classes of problems in differential equations [38–41].

To the best of our knowledge, there is no result in the literature on the collocation

method based on exponential B-spline functions for the time-fractional Black-Scholes model. So, we propose an effective collocation technique to solve the time-fractional Black-Scholes problem numerically. To achieve this we use exponential B-spline functions to discretize the space derivative and apply a finite difference method to discretize the Caputo fractional derivative. It is proved that the method is unconditionally stable by means of von Neumann analysis. Further, it is shown that the proposed method is convergent of order  $O(h_x^2, h_t^{2-\mu})$ , where  $h_t$  and  $h_x$  represent mesh spacing in the time and space directions, respectively. We perform several numerical experiments to validate the theoretical findings. We use the proposed method to price three European options governed by a TFBSM, namely the European call option, the European put option, and the European double barrier knock-out call option. In addition, we examine how the order of time-fractional derivative affects the option price.

The remaining paper is as structured follows. Section 2 describes the model problem. Section 3 is devoted to the proposed numerical method. The stability and convergence of the method are discussed in Sections 4 and 5 respectively. To validate our theoretical findings, several numerical examples are considered in Section 6. Finally, the paper is concluded in Section 7.

## 2. The model problem

Consider the following time-fractional Black-Scholes model (TFBSM) [16] that expresses the option price problem

$$\frac{\partial^\mu \mathcal{V}(\xi, \tau)}{\partial \tau^\mu} + \frac{\sigma^2 \xi^2}{2} \frac{\partial^2 \mathcal{V}(\xi, \tau)}{\partial \xi^2} + r_f \xi \frac{\partial \mathcal{V}(\xi, \tau)}{\partial \xi} - r_f \mathcal{V}(\xi, \tau) = 0, \quad (\xi, \tau) \in \mathbb{R}^+ \times (0, \tilde{T}), \quad (3)$$

with

$$\begin{cases} \mathcal{V}(\xi, \tilde{T}) = \phi(\xi), \\ \mathcal{V}(0, \tau) = \mathcal{H}(\tau), \\ \mathcal{V}(\infty, \tau) = \mathcal{G}(\tau), \end{cases} \quad (4)$$

where  $0 < \mu \leq 1$  and all other notations are same as defined for problem (1). Further, the modified Riemann-Liouville fractional time derivative is defined by [42]

$$\frac{\partial^\mu \mathcal{V}(\xi, \tau)}{\partial \tau^\mu} = \begin{cases} \frac{1}{\Gamma(1-\mu)} \frac{d}{d\tau} \int_\tau^{\tilde{T}} \frac{\mathcal{V}(\xi, \nu) - \mathcal{V}(\xi, \tilde{T})}{(\nu - \tau)^\mu} d\nu, & 0 < \mu < 1, \\ \frac{\partial \mathcal{V}}{\partial \tau} & \mu = 1. \end{cases} \quad (5)$$

When  $\mu = 1$ , the model (3)-(4) converts to the classical Black-Scholes model (1)-(2).

We consider the transformation  $\tau = \tilde{T} - t$ , for  $0 < \mu < 1$ , and proceed as follows

$$\begin{aligned}
\frac{\partial^\mu \mathcal{V}(\xi, \tau)}{\partial \tau^\mu} &= \frac{1}{\Gamma(1-\mu)} \frac{d}{d\tau} \int_\tau^{\tilde{T}} \frac{\mathcal{V}(\xi, \nu) - \mathcal{V}(\xi, \tilde{T})}{(\nu - \tau)^\mu} d\nu \\
&= \frac{-1}{\Gamma(1-\mu)} \frac{d}{dt} \int_{\tilde{T}-t}^{\tilde{T}} \frac{\mathcal{V}(\xi, \nu) - \mathcal{V}(\xi, \tilde{T})}{(\nu - \tilde{T} + t)^\mu} d\nu \\
&= \frac{-1}{\Gamma(1-\mu)} \frac{d}{dt} \int_0^t \frac{\mathcal{V}(\xi, \tilde{T} - \tilde{\xi}) - \mathcal{V}(\xi, \tilde{T})}{(t - \tilde{\xi})^\mu} d\tilde{\xi} \quad (\text{using } \nu = \tilde{T} - \tilde{\xi}) \\
&= \frac{-1}{\Gamma(1-\mu)} \frac{d}{dt} \int_0^t \frac{u(\varkappa, \tilde{\xi}) - u(\varkappa, 0)}{(t - \tilde{\xi})^\mu} d\tilde{\xi}.
\end{aligned}$$

Now defining

$${}_0D_t^\mu u(\varkappa, t) = \frac{1}{\Gamma(1-\mu)} \frac{d}{dt} \int_0^t \frac{u(\varkappa, \tilde{\xi}) - u(\varkappa, 0)}{(t - \tilde{\xi})^\mu} d\tilde{\xi}, \quad (0 < \mu < 1),$$

we have

$$\frac{\partial^\mu \mathcal{V}(\xi, \tau)}{\partial \tau^\mu} = -{}_0D_t^\mu u(\varkappa, t).$$

Therefore, letting  $\xi = e^x$  and denoting  $u(\varkappa, t) = \mathcal{V}(e^\varkappa, \tilde{T} - t)$ , we rewrite (3)-(4) as follows

$${}_0D_t^\mu u(\varkappa, t) = \frac{\sigma^2}{2} \frac{\partial^2 u(\varkappa, t)}{\partial \varkappa^2} + \left(r_f - \frac{\sigma^2}{2}\right) \frac{\partial u(\varkappa, t)}{\partial \varkappa} - r_f u(\varkappa, t), \quad (\varkappa, t) \in \mathbb{R} \times (0, \tilde{T}), \quad (6)$$

with

$$\begin{cases} u(\varkappa, 0) = z(\varkappa), \\ u(-\infty, t) = \mathcal{H}(t), \\ u(\infty, t) = \mathcal{G}(t). \end{cases} \quad (7)$$

The modified Riemann-Liouville fractional time derivative operator  ${}_0D_t^\mu$  can be transformed into the Caputo fractional time derivative operator  ${}_0^C D_t^\mu$  for  $0 < \mu \leq 1$  following

[21]:

$$\begin{aligned}
{}_0D_t^\mu u(\varkappa, t) &= \frac{1}{\Gamma(1-\mu)} \frac{d}{dt} \int_0^t \frac{u(\varkappa, \tilde{\xi}) - u(\varkappa, 0)}{(t-\tilde{\xi})^\mu} d\tilde{\xi}, \\
&= \frac{1}{\Gamma(1-\mu)} \frac{d}{dt} \int_0^t \frac{u(\varkappa, \tilde{\xi})}{(t-\tilde{\xi})^\mu} d\tilde{\xi} - \frac{1}{\Gamma(1-\mu)} \frac{d}{dt} \int_0^t \frac{u(\varkappa, 0)}{(t-\tilde{\xi})^\mu} d\tilde{\xi}, \\
&= \frac{1}{\Gamma(1-\mu)} \frac{d}{dt} \int_0^t \frac{u(\varkappa, \tilde{\xi})}{(t-\tilde{\xi})^\mu} d\tilde{\xi} - \frac{t^{-\mu}}{\Gamma(1-\mu)} u(\varkappa, 0), \\
&= \frac{1}{\Gamma(1-\mu)} \int_0^t (t-\tilde{\xi})^{-\mu} \frac{\partial u(\varkappa, \tilde{\xi})}{\partial \tilde{\xi}} d\tilde{\xi}, \\
&= {}_0^C D_t^\mu u(\varkappa, t).
\end{aligned}$$

Lastly, to solve the problem numerically, we need to truncate the unbounded domain into a finite interval  $(I_p, F_p)$ . Also, without loss of generality we add a source term to the RHS of the equation (6). Thus, we have the following problem

$${}_0^C D_t^\mu u(\varkappa, t) = \alpha \frac{\partial^2 u(\varkappa, t)}{\partial \varkappa^2} + \beta \frac{\partial u(\varkappa, t)}{\partial x} - \gamma u(\varkappa, t) + \psi(\varkappa, t), \quad (\varkappa, t) \in (I_p, F_p) \times (0, \tilde{T}), \quad (8)$$

with

$$\begin{cases} u(\varkappa, 0) = z(\varkappa), \\ u(I_p, t) = \mathcal{H}(t), \\ u(F_p, t) = \mathcal{G}(t), \end{cases} \quad (9)$$

where  $\alpha = \frac{\sigma^2}{2} > 0$ ,  $\beta = r_f - \frac{\sigma^2}{2}$ , and  $\gamma = r_f > 0$ . From the above fractional Black-Scholes model, we can obtain the widely known reaction-diffusion model by taking  $\alpha > 0$ ,  $\beta = 0$ , and  $\gamma \neq 0$ , and the time fractional advection-diffusion model by taking  $\alpha > 0$ ,  $\beta < 0$ , and  $\gamma = 0$ . One find several works for both the models, but from the existing literature, it seems that the work on the time-fractional Black-Scholes model is comparatively less and confined. Therefore, in this paper, we have considered the time-fractional Black-Scholes model to solve it numerically using the collocation method based on the exponential B-spline functions.

### 3. Numerical Scheme

#### 3.1. Outline of the Exponential B-spline functions

Let  $\Pi_\varkappa : I_p = \varkappa_0 < \varkappa_1 < \dots < \varkappa_{N_\varkappa-1} < \varkappa_{N_\varkappa} = F_p$  be the uniform partition of  $[I_p, F_p]$  with  $\varkappa_m = I_p + mh_\varkappa$ , where  $m = 0, 1, 2, \dots, N_\varkappa$ , and  $h_\varkappa = \frac{(F_p - I_p)}{N_\varkappa}$  is the mesh spacing in space direction. Suppose

$$\begin{aligned} \tilde{s} &= \sinh(\rho h_\varkappa), \\ \tilde{c} &= \cosh(\rho h_\varkappa), \end{aligned}$$

Table 1: The values of  $\mathcal{Q}_m(\varkappa)$ ,  $\mathcal{Q}'_m(\varkappa)$ , and  $\mathcal{Q}''_m(\varkappa)$  at each mesh point.

	$\mathcal{Q}_m(\varkappa_i)$	$\mathcal{Q}'_m(\varkappa_i)$	$\mathcal{Q}''_m(\varkappa_i)$
$i = m$	1	0	$\frac{-\rho^2 \tilde{s}}{\rho h_\varkappa \tilde{c} - \tilde{s}}$
$i = m \pm 1$	$\frac{\tilde{s} - \rho h_\varkappa}{2(\rho h_\varkappa \tilde{c} - \tilde{s})}$	$\frac{\mp \rho(\tilde{c} - 1)}{2(\rho h_\varkappa \tilde{c} - \tilde{s})}$	$\frac{\rho^2 \tilde{s}}{2(\rho h_\varkappa \tilde{c} - \tilde{s})}$
else	0	0	0

where  $\rho$  is a non-negative tension parameter. A generalization of the cubic spline as an exponential spline has been proposed by McCartin [37]. The presence of non-negative tension parameter plays an important role in the exponential spline and it accommodates the stiffness of multiple spline segments. The exponential B-spline functions are defined on the above mentioned partition  $\Pi_\varkappa$  along with six more points  $\varkappa_i$ , where  $i = -3, -2, -1, N_\varkappa + 1, N_\varkappa + 2, N_\varkappa + 3$ , which are outside of the interval  $[I_p, F_p]$ . The exponential B-spline functions  $\mathcal{Q}_m(\varkappa)$  are defined as follows

$$\mathcal{Q}_m(\varkappa) = \begin{cases} \tilde{r}(\varkappa_{m-2} - \varkappa) - \frac{\tilde{r}}{\rho} \sinh(\rho(\varkappa_{m-2} - \varkappa)), & \varkappa \in [\varkappa_{m-2}, \varkappa_{m-1}], \\ \tilde{a} + \tilde{b}(\varkappa_m - \varkappa) + \tilde{c}e^{\rho(\varkappa_m - \varkappa)} + qe^{-\rho(\varkappa_m - \varkappa)}, & \varkappa \in [\varkappa_{m-1}, \varkappa_m], \\ \tilde{a} + \tilde{b}(\varkappa - \varkappa_m) + \tilde{c}e^{\rho(\varkappa - \varkappa_m)} + qe^{-\rho(\varkappa - \varkappa_m)}, & \varkappa \in [\varkappa_m, \varkappa_{m+1}], \\ \tilde{r}(\varkappa - \varkappa_{m+2}) - \frac{\tilde{r}}{\rho} \sinh(\rho(\varkappa - \varkappa_{m+2})), & \varkappa \in [\varkappa_{m+1}, \varkappa_{m+2}], \\ 0, & \text{otherwise,} \end{cases} \quad (10)$$

where  $m = -1, 0, \dots, N_\varkappa, N_\varkappa + 1$ , and

$$\begin{aligned} \tilde{r} &= \frac{\rho}{2(\rho h_\varkappa \tilde{c} - \tilde{s})}, & \tilde{a} &= \frac{\rho h_\varkappa \tilde{c}}{\rho h_\varkappa \tilde{c} - \tilde{s}}, & \tilde{b} &= \frac{\rho}{2} \left[ \frac{\tilde{c}(\tilde{c} - 1) + \tilde{s}^2}{(\rho h_\varkappa \tilde{c} - \tilde{s})(1 - \tilde{c})} \right], \\ \tilde{c} &= \frac{1}{4} \left[ \frac{e^{-\rho h_\varkappa}(1 - \tilde{c}) + \tilde{s}(e^{-\rho h_\varkappa} - 1)}{(\rho h_\varkappa \tilde{c} - \tilde{s})(1 - \tilde{c})} \right], \\ q &= \frac{1}{4} \left[ \frac{e^{\rho h_\varkappa}(\tilde{c} - 1) + \tilde{s}(e^{\rho h_\varkappa} - 1)}{(\rho h_\varkappa \tilde{c} - \tilde{s})(1 - \tilde{c})} \right]. \end{aligned}$$

The exponential B-spline functions  $\mathcal{Q}_{-1}(\varkappa)$ ,  $\mathcal{Q}_0(\varkappa)$ ,  $\dots$ ,  $\mathcal{Q}_{N_\varkappa}(\varkappa)$ , and  $\mathcal{Q}_{N_\varkappa+1}(\varkappa)$  are twice continuously differentiable over  $\mathbb{R}$  and have local support. The set  $\{\mathcal{Q}_m(\varkappa)\}_{m=-1}^{N_\varkappa+1}$  is linearly independent and forms a basis for the exponential B-spline space  $\mathcal{W}_{N_\varkappa+3} = \text{span}(\{\mathcal{Q}_m(\varkappa)\}_{m=-1}^{N_\varkappa+1})$  over the interval  $[I_p, F_p]$ . The values of  $\mathcal{Q}_m(\varkappa)$ ,  $\mathcal{Q}'_m(\varkappa)$ , and  $\mathcal{Q}''_m(\varkappa)$  at each mesh point are given in the Table 1.

### 3.2. A fully discrete numerical scheme

In this sub-section, first we will discretize the Caputo time-fractional derivative and then derive the fully-discretized numerical scheme. Let  $\Pi_t : 0 = t_0 < t_1 < \dots < t_{N_t-1} < t_{N_t} = \tilde{T}$  be the uniform partition of  $[0, \tilde{T}]$ , where  $t_n = nh_t$ ,  $n = 0, 1, 2, \dots, N_t$ , with  $h_t = \frac{\tilde{T}}{N_t}$

is the mesh spacing in the time direction. We approximate the Caputo time fractional derivative  ${}_0^C D_t^\mu u(\boldsymbol{x}, t)$  at  $t_{n+1}$ ,  $n = -1, 0, \dots, N_t - 1$ , using  $L1$  method [43] as follows

$$\begin{aligned} {}_0^C D_t^\mu u(\boldsymbol{x}, t_{n+1}) &= \frac{1}{\Gamma(1-\mu)} \int_0^{t_{n+1}} (t_{n+1} - s)^{-\mu} \frac{\partial u}{\partial s}(\boldsymbol{x}, s) ds \\ &= \frac{1}{\Gamma(1-\mu)} \sum_{k=0}^n \int_{t_k}^{t_{k+1}} (t_{n+1} - s)^{-\mu} \left[ \frac{u(\boldsymbol{x}, t_{k+1}) - u(\boldsymbol{x}, t_k)}{h_t} \right] ds + R^{n+1} \\ &= \frac{h_t^{-\mu}}{\Gamma(2-\mu)} \sum_{k=0}^n w_k [u(\boldsymbol{x}, t_{n-k+1}) - u(\boldsymbol{x}, t_{n-k})] + R_1^{n+1}, \end{aligned} \quad (11)$$

where  $w_k = (k+1)^{1-\mu} - k^{1-\mu}$  and the truncation error  $R_1^{n+1}$  is bounded by

$$|R^{n+1}| \leq k_1 h_t^{2-\mu}, \quad (12)$$

where  $k_1$  is a constant.

**Lemma 3.1.** *The coefficients  $w_k$  satisfy [44]*

- (a).  $w_0 = 1$ ,
- (b).  $w_k > 0$ ,  $0 \leq k \leq n$ ,
- (c).  $\langle w_k \rangle$  is monotonic decreasing sequence,
- (d).  $\sum_{k=0}^n (w_k - w_{k+1}) + w_{n+1} = 1$ .

At time level  $n+1$ , the equation (8) takes the form

$${}_0^C D_t^\mu u(\boldsymbol{x}, t_{n+1}) = \alpha \frac{\partial^2 u^{n+1}(\boldsymbol{x})}{\partial \boldsymbol{x}^2} + \beta \frac{\partial u^{n+1}(\boldsymbol{x})}{\partial x} - \gamma u^{n+1}(\boldsymbol{x}) + \psi^{n+1}(\boldsymbol{x}). \quad (13)$$

Now we discretize equation (13). Substitution of equation (11) in equation (13) gives

$$\sum_{k=0}^n w_k [u(\boldsymbol{x}, t_{n-k+1}) - u(\boldsymbol{x}, t_{n-k})] + R^{n+1} = \alpha \tilde{\gamma} \frac{\partial^2 u^{n+1}(\boldsymbol{x})}{\partial \boldsymbol{x}^2} + \beta \tilde{\gamma} \frac{\partial u^{n+1}(\boldsymbol{x})}{\partial \boldsymbol{x}} - \gamma \tilde{\gamma} u^{n+1}(\boldsymbol{x}) + \tilde{\gamma} \psi^{n+1}(\boldsymbol{x}), \quad (14)$$

$$(-1 \leq n \leq N_t - 1),$$

where

$$\tilde{\gamma} = \Gamma(2-\mu) h_t^\mu.$$

The initial and boundary conditions in (9) result in

$$\begin{cases} u^0(\boldsymbol{x}) = z(\boldsymbol{x}), \\ u^{n+1}(I_p) = \mathcal{H}(t_{n+1}), & -1 \leq n \leq N_t - 1, \\ u^{n+1}(F_p) = \mathcal{G}(t_{n+1}), & -1 \leq n \leq N_t - 1. \end{cases} \quad (15)$$

The approximate solution  $\mathcal{U}^{n+1}(\boldsymbol{x})$  to the analytical solution  $u^{n+1}(\boldsymbol{x})$  of problem (8)-(9)

is considered to be in the following form

$$\mathcal{U}^{n+1}(\boldsymbol{x}) = \sum_{m=-1}^{N_{\boldsymbol{x}}+1} \mathcal{R}_m^{n+1} \mathcal{Q}_m(\boldsymbol{x}), \quad (16)$$

where  $\mathcal{R}_m^{n+1}$  are unknown coefficients that need to be determined. With the help of Table 1 we can obtain  $\mathcal{U}^{n+1}(\boldsymbol{x}_m)$ ,  $\mathcal{U}_{\boldsymbol{x}}^{n+1}(\boldsymbol{x}_m)$ , and  $\mathcal{U}_{\boldsymbol{x}\boldsymbol{x}}^{n+1}(\boldsymbol{x}_m)$ , for  $-1 \leq m \leq N_{\boldsymbol{x}} + 1$ , in terms of the coefficients  $\mathcal{R}_m^{n+1}$  as follows

$$\mathcal{U}^{n+1}(\boldsymbol{x}_m) = \eta \mathcal{R}_{m-1}^{n+1} + \mathcal{R}_m^{n+1} + \eta \mathcal{R}_{m+1}^{n+1}, \quad (17)$$

$$\mathcal{U}_{\boldsymbol{x}}^{n+1}(\boldsymbol{x}_m) = \tilde{e}(\tilde{c} - 1)[\mathcal{R}_{m+1}^{n+1} - \mathcal{R}_{m-1}^{n+1}], \quad (18)$$

$$\mathcal{U}_{\boldsymbol{x}\boldsymbol{x}}^{n+1}(\boldsymbol{x}_m) = \bar{\eta}[\mathcal{R}_{m-1}^{n+1} - 2\mathcal{R}_m^{n+1} + \mathcal{R}_{m+1}^{n+1}], \quad (19)$$

where

$$\eta = \frac{\tilde{s} - \rho h_{\boldsymbol{x}}}{2(\rho h_{\boldsymbol{x}} \tilde{c} - \tilde{s})}, \quad \tilde{e} = \frac{\rho}{2(\rho h_{\boldsymbol{x}} \tilde{c} - \tilde{s})}, \quad \bar{\eta} = \frac{\rho^2 \tilde{s}}{2(\rho h_{\boldsymbol{x}} \tilde{c} - \tilde{s})}.$$

Now the discretization of (14) at  $\boldsymbol{x} = \boldsymbol{x}_m$  gives

$$\begin{aligned} \sum_{k=0}^n w_k [u(\boldsymbol{x}_m, t_{n-k+1}) - u(\boldsymbol{x}_m, t_{n-k})] + R^{n+1} &= \alpha \tilde{\gamma} \frac{\partial^2 u^{n+1}(\boldsymbol{x}_m)}{\partial \boldsymbol{x}_m^2} + \beta \tilde{\gamma} \frac{\partial u^{n+1}(\boldsymbol{x}_m)}{\partial \boldsymbol{x}_m} - \gamma \tilde{\gamma} u^{n+1}(\boldsymbol{x}_m) \\ &\quad + \tilde{\gamma} \psi^{n+1}(\boldsymbol{x}_m), \end{aligned} \quad (0 \leq m \leq N_{\boldsymbol{x}}, -1 \leq n \leq N_t - 1), \quad (20)$$

The exponential B-spline function  $\mathcal{U}^{n+1}(\boldsymbol{x})$  satisfies the collocation conditions as follows

$$\begin{aligned} \sum_{k=0}^n w_k [\mathcal{U}^{n-k+1}(\boldsymbol{x}_m) - \mathcal{U}^{n-k}(\boldsymbol{x}_m)] &= \alpha \tilde{\gamma} \frac{\partial^2 \mathcal{U}^{n+1}(\boldsymbol{x}_m)}{\partial \boldsymbol{x}^2} + \beta \tilde{\gamma} \frac{\partial \mathcal{U}^{n+1}(\boldsymbol{x}_m)}{\partial \boldsymbol{x}} - \gamma \tilde{\gamma} \mathcal{U}^{n+1}(\boldsymbol{x}_m) \\ &\quad + \tilde{\gamma} \psi^{n+1}(\boldsymbol{x}_m), \end{aligned} \quad (0 \leq m \leq N_{\boldsymbol{x}}, -1 \leq n \leq N_t - 1) \quad (21)$$

$$\begin{cases} \mathcal{U}^0(\boldsymbol{x}_m) = z_m, \\ \mathcal{U}^{n+1}(\boldsymbol{x}_0) = \mathcal{H}_{n+1}, & -1 \leq n \leq N_t - 1, \\ \mathcal{U}^{n+1}(\boldsymbol{x}_{N_{\boldsymbol{x}}}) = \mathcal{G}_{n+1}, & -1 \leq n \leq N_t - 1, \end{cases} \quad (22)$$

where  $z(\boldsymbol{x}_m) = z_m$ ,  $\mathcal{H}(t_{n+1}) = \mathcal{H}_{n+1}$ , and  $\mathcal{G}(t_{n+1}) = \mathcal{G}_{n+1}$ .

Now the substitution of the equations (17), (18), and (19) in equation (21), and the substitution of equation (17) in boundary conditions given in equation (22) yield



$$\chi_1 \mathcal{R}_{m-1}^{n+1} + \chi_2 \mathcal{R}_m^{n+1} + \chi_3 \mathcal{R}_{m+1}^{n+1} = \eta \mathcal{R}_{m-1}^n + \mathcal{R}_m^n + \eta \mathcal{R}_{m+1}^n - \sum_{k=1}^n w_k [(\eta \mathcal{R}_{m-1}^{n-k+1} + \mathcal{R}_m^{n-k+1} + \eta \mathcal{R}_{m+1}^{n-k+1}) - (\eta \mathcal{R}_{m-1}^{n-k} + \mathcal{R}_m^{n-k} + \eta \mathcal{R}_{m+1}^{n-k})] + \tilde{\gamma} \psi^{n+1}(\mathcal{R}_m), \quad (23)$$

and

$$\eta \mathcal{R}_{-1}^{n+1} = \mathcal{H}_{n+1} - \mathcal{R}_0^{n+1} - \eta \mathcal{R}_1^{n+1}, \quad (24)$$

$$\eta \mathcal{R}_{N_\varepsilon+1}^{n+1} = \mathcal{G}_{n+1} - \mathcal{R}_{N_\varepsilon}^{n+1} - \eta \mathcal{R}_{N_\varepsilon-1}^{n+1}, \quad (25)$$

where

$$\chi_1 = \eta - \alpha \tilde{\gamma} \bar{\eta} + \beta \tilde{\gamma} \bar{e} (\bar{c} - 1) + \eta \gamma \tilde{\gamma},$$

$$\chi_2 = 1 + 2\alpha \tilde{\gamma} \bar{\eta} + \gamma \tilde{\gamma},$$

$$\chi_3 = \eta - \alpha \tilde{\gamma} \bar{\eta} - \beta \tilde{\gamma} \bar{e} (\bar{c} - 1) + \eta \gamma \tilde{\gamma}.$$

From the system (23) the unknown coefficients  $\mathcal{R}_{-1}^{n+1}$  and  $\mathcal{R}_{N_\varepsilon+1}^{n+1}$  can be eliminated using the equations (24) and (25) respectively. Finally, we get for each  $n$  a tri-diagonal system of  $(N_\varepsilon+1)$  equations in  $(N_\varepsilon+1)$  unknowns which can be solved by the Thomas algorithm. We have

$$S \mathcal{R}^{n+1} = Q \left( \mathcal{R}^n - \sum_{k=1}^n w_k (\mathcal{R}^{n-k+1} - \mathcal{R}^{n-k}) \right) + B, \quad (26)$$

where

$$S = \begin{pmatrix} \mathcal{E}_1 & \mathcal{E}_2 & 0 & 0 & \dots & 0 & 0 & 0 & 0 \\ \chi_1 & \chi_2 & \chi_3 & 0 & \dots & 0 & 0 & 0 & 0 \\ 0 & \chi_1 & \chi_2 & \chi_3 & \dots & 0 & 0 & 0 & 0 \\ & & & & \dots & & & & \\ 0 & 0 & 0 & 0 & \dots & \chi_1 & \chi_2 & \chi_3 & 0 \\ 0 & 0 & 0 & 0 & \dots & 0 & \chi_1 & \chi_2 & \chi_3 \\ 0 & 0 & 0 & 0 & \dots & 0 & 0 & -\mathcal{E}_2 & \mathcal{E}_3 \end{pmatrix},$$

$$\mathcal{R}^n = \begin{pmatrix} \mathcal{R}_0^n \\ \mathcal{R}_1^n \\ \vdots \\ \vdots \\ \mathcal{R}_{M-1}^n \\ \mathcal{R}_M^n \end{pmatrix}, \quad Q = \begin{pmatrix} 0 & 0 & 0 & 0 & \dots & 0 & 0 & 0 & 0 \\ \eta & 1 & \eta & 0 & \dots & 0 & 0 & 0 & 0 \\ 0 & \eta & 1 & \eta & \dots & 0 & 0 & 0 & 0 \\ & & & & \dots & & & & \\ 0 & 0 & 0 & 0 & \dots & \eta & 1 & \eta & 0 \\ 0 & 0 & 0 & 0 & \dots & 0 & \eta & 1 & \eta \\ 0 & 0 & 0 & 0 & \dots & 0 & 0 & 0 & 0 \end{pmatrix},$$

$$\begin{aligned}
\mathcal{E}_1 &= \alpha\tilde{\gamma}\tilde{\eta} \left( 2 + \frac{1}{\eta} \right) - \frac{\beta\tilde{\gamma}\tilde{e}(\tilde{c} - 1)}{\eta}, \\
\mathcal{E}_2 &= -2\beta\tilde{\gamma}\tilde{e}(\tilde{c} - 1), \\
\mathcal{E}_3 &= \alpha\tilde{\gamma}\tilde{\eta} \left( 2 + \frac{1}{\eta} \right) + \frac{\beta\tilde{\gamma}\tilde{e}(\tilde{c} - 1)}{\eta},
\end{aligned}$$

and

$$B = \begin{pmatrix} \mathcal{H}_n - \sum_{k=1}^n w_k(\mathcal{H}_{n-k+1} - \mathcal{H}_{n-k}) - \frac{\chi_1}{\eta}\mathcal{H}_{n+1} + \tilde{\gamma}\psi^{n+1}(\boldsymbol{x}_0) \\ \tilde{\gamma}\psi^{n+1}(\boldsymbol{x}_1) \\ \tilde{\gamma}\psi^{n+1}(\boldsymbol{x}_2) \\ \vdots \\ \tilde{\gamma}\psi^{n+1}(\boldsymbol{x}_{N_\varkappa-1}) \\ \mathcal{G}_n - \sum_{k=1}^n w_k(\mathcal{G}_{n-k+1} - \mathcal{G}_{n-k}) - \frac{\chi_3}{\eta}\mathcal{G}_{n+1} + \tilde{\gamma}\psi^{n+1}(\boldsymbol{x}_{N_\varkappa}) \end{pmatrix}.$$

We observe that the set of systems in (26) for  $n = 0, 1, \dots, N_t$ , can be solved recursively if we know the initial vector  $\mathcal{R}^0$ . Note that  $\mathcal{R}_{-1}^0$  and  $\mathcal{R}_{N_\varkappa+1}^0$  can be then calculated using equations (24) and (25) respectively.

### 3.3. Initial state

To start the process, an appropriate initial vector  $\mathcal{R}^0$  is needed for the system. For this, we consider the initial conditions in (22),

$$\mathcal{U}_\varkappa^0(I_p) = z'(I_p), \quad \mathcal{U}_\varkappa^0(F_p) = z'(F_p).$$

Now substituting the relation (18) in the above two equations we get

$$\mathcal{U}_\varkappa^0(\boldsymbol{x}_0) = \mathcal{U}_\varkappa^0(I_p) = \tilde{e}(\tilde{c} - 1)[\mathcal{R}_1^0 - \mathcal{R}_{-1}^0] = z'(I_p), \quad (27)$$

$$\mathcal{U}_\varkappa^0(\boldsymbol{x}_{N_\varkappa}) = \mathcal{U}_\varkappa^0(F_p) = \tilde{e}(\tilde{c} - 1)[\mathcal{R}_{N_\varkappa+1}^0 - \mathcal{R}_{N_\varkappa-1}^0] = z'(F_p). \quad (28)$$

Further, the relation (17) with the initial condition in (22), yields an algebraic system of  $(N_\varkappa + 1)$  equations

$$\mathcal{U}^0(\boldsymbol{x}_m) = \eta\mathcal{R}_{m-1}^0 + \mathcal{R}_m^0 + \eta\mathcal{R}_{m+1}^0 = z_m, \quad m = 0, 1, \dots, N_\varkappa, \quad (29)$$

with unknowns  $\mathcal{R}_{-1}^0, \mathcal{R}_0^0, \mathcal{R}_1^0, \dots, \mathcal{R}_{N_\varkappa-1}^0, \mathcal{R}_{N_\varkappa}^0, \mathcal{R}_{N_\varkappa+1}^0$ . Here,  $\mathcal{R}_{-1}^0$  and  $\mathcal{R}_{N_\varkappa+1}^0$  can be removed using equations (27) and (28) respectively. Thus, we get a tridiagonal system of size  $(N_\varkappa + 1) \times (N_\varkappa + 1)$  which can also be solved using the Thomas algorithm. We have

$$T\mathcal{R}^0 = \mathcal{C}, \quad (30)$$

where

$$T = \begin{pmatrix} 1 & 2\eta & 0 & 0 & \dots & 0 & 0 & 0 & 0 \\ \eta & 1 & \eta & 0 & \dots & 0 & 0 & 0 & 0 \\ 0 & \eta & 1 & \eta & \dots & 0 & 0 & 0 & 0 \\ & & & & \dots & & & & \\ 0 & 0 & 0 & 0 & \dots & \eta & 1 & \eta & 0 \\ 0 & 0 & 0 & 0 & \dots & 0 & \eta & 1 & \eta \\ 0 & 0 & 0 & 0 & \dots & 0 & 0 & 2\eta & 1 \end{pmatrix},$$

$$\mathcal{R}^0 = \begin{pmatrix} \mathcal{R}_0^0 \\ \mathcal{R}_1^0 \\ \vdots \\ \vdots \\ \mathcal{R}_{N_x-1}^0 \\ \mathcal{R}_{N_x}^0 \end{pmatrix}, \quad \mathcal{C} = \begin{pmatrix} z_0 + \frac{\eta}{\bar{e}(\bar{e}-1)} z'(I_p) \\ z_1 \\ \vdots \\ \vdots \\ z_{N_x-1} \\ z_{N_x} - \frac{\eta}{\bar{e}(\bar{e}-1)} z'(F_p) \end{pmatrix}.$$

#### 4. Stability analysis

In this section we discuss the stability analysis of the proposed scheme.

**Theorem 4.1.** *The numerical scheme (23) solving the TFBSM (8)-(9) is unconditionally stable.*

*Proof.* Let  $\bar{\mathcal{R}}$  be a perturbed solution of the system (23). We will investigate how the perturbation  $\delta_m^n = \mathcal{R}_m^n - \bar{\mathcal{R}}_m^n$  develops over time. Note that  $\delta_m^n$  solves the following equation

$$\begin{aligned} \chi_1 \delta_{m-1}^{n+1} + \chi_2 \delta_m^{n+1} + \chi_3 \delta_{m+1}^{n+1} = & \eta \delta_{m-1}^n + \delta_m^n + \eta \delta_{m+1}^n - \sum_{k=1}^n w_k [(\eta \delta_{m-1}^{n-k+1} + \delta_m^{n-k+1} + \eta \delta_{m+1}^{n-k+1}) \\ & - (\eta \delta_{m-1}^{n-k} + \delta_m^{n-k} + \eta \delta_{m+1}^{n-k})]. \end{aligned} \quad (31)$$

Now, to use the von Neumann stability analysis we assume that

$$\delta_m^n = \zeta^n e^{i\omega m h_x}, \quad (32)$$

where  $i = \sqrt{-1}$  and  $\omega$  is the wave number. Inserting the equation (32) in (31) yields

$$\zeta^{n+1} = \frac{\Upsilon_1}{(\Upsilon_1 + \Upsilon_2 + \Upsilon_3 - i\Upsilon_4)} \left[ \zeta^n - \sum_{k=1}^n w_k (\zeta^{n-k+1} - \zeta^{n-k}) \right], \quad (33)$$

where

$$\begin{aligned}\Upsilon_1 &= 1 + 2\eta \cos \omega h_{\varkappa}, & \Upsilon_2 &= 2\alpha\tilde{\gamma}\tilde{\eta}(1 - \cos \omega h_{\varkappa}), \\ \Upsilon_3 &= \gamma\tilde{\gamma}(1 + 2\eta \cos \omega h_{\varkappa}), & \text{and} & \quad \Upsilon_4 = 2\beta\tilde{\gamma}\tilde{e}(\tilde{c} - 1) \sin \omega h_{\varkappa}.\end{aligned}$$

From equation (33), we have

$$|\zeta^{n+1}|^2 \leq \frac{|\Upsilon_1|^2}{((\Upsilon_1 + \Upsilon_2 + \Upsilon_3)^2 + \Upsilon_4^2)} \left| \left[ \zeta^n - \sum_{k=1}^n w_k (\zeta^{n-k+1} - \zeta^{n-k}) \right] \right|^2. \quad (34)$$

Since  $|\Upsilon_1|^2 < (\Upsilon_1 + \Upsilon_2 + \Upsilon_3)^2 + \Upsilon_4^2$ , the equation (34) takes the form

$$|\zeta^{n+1}| \leq \left| \left[ \zeta^n - \sum_{k=1}^n w_k (\zeta^{n-k+1} - \zeta^{n-k}) \right] \right|. \quad (35)$$

To show  $|\zeta^{n+1}| \leq |\zeta^0|$ , the mathematical induction is used. For  $n = 0$  in equation (35) we have  $|\zeta^1| \leq |\zeta^0|$ . Further, we assume that

$$|\zeta^j| \leq |\zeta^0|, \quad j = 1, 2, \dots, n. \quad (36)$$

Now from the equation (35) and using the assumptions in (36) and Lemma 3.1 we have

$$|\zeta^{n+1}| \leq \left| \left[ w_n \zeta^0 + \sum_{k=0}^{n-1} (w_k - w_{k+1}) \zeta^{n-k} \right] \right| \leq \left[ w_n + \sum_{k=0}^{n-1} (w_k - w_{k+1}) \right] |\zeta^0| = |\zeta^0|.$$

Hence, the inequality (36) holds for all  $n$ . Thus, we observe that the perturbation is bounded at each time level and therefore the numerical scheme (23) solving the TFBSM (8)-(9) is unconditionally stable. This completes the proof.  $\square$

## 5. Convergence analysis

We now discuss the convergence analysis of the numerical scheme (23). We shall use the following results.

**Lemma 5.1.** *The basis elements  $\{\mathcal{Q}_m(\varkappa)\}_{m=-1}^{N_{\varkappa}+1}$  of the exponential B-spline space  $\mathcal{W}_{N_{\varkappa}+3}$  satisfy the following inequality*

$$\sum_{m=-1}^{N_{\varkappa}+1} |\mathcal{Q}_m(\varkappa)| \leq \frac{5}{2}, \quad I_p \leq \varkappa \leq F_p.$$

*Proof.* See [38, Lemma 4.1] for the proof.  $\square$

**Theorem 5.2.** *Let the exact solution  $u^{n+1}(\varkappa)$  of problem (8)-(9) be interpolated by a unique exponential B-spline  $\tilde{V}^{n+1}(\varkappa)$  in  $\mathcal{W}_{N_{\varkappa}+3}$ . If  $u \in C^{4,0}[0, 1]$  and  $\psi \in C^{2,0}[0, 1]$ , then*

there exists positive constants  $c_i$  such that

$$\left\| \frac{\partial^i}{\partial \mathcal{X}^i} \left( u^{n+1}(\mathcal{X}) - \tilde{V}^{n+1}(\mathcal{X}) \right) \right\|_{\infty} \leq c_i h_{\mathcal{X}}^{4-i}, \quad i = 0, 1, 2.$$

*Proof.* See [35] for the proof.  $\square$

**Theorem 5.3.** Let  $\mathcal{U}^{n+1}(\mathcal{X})$  be the collocation approximation in (16) from the exponential B-spline space  $\mathcal{W}_{N_{\mathcal{X}}+3}$  to the exact solution  $u^{n+1}(\mathcal{X})$  of the TFBSM (8)-(9). If  $u \in C^{4,0}[0, 1]$  and  $\psi \in C^{2,0}[0, 1]$ , then there exists a positive constant  $\lambda^*$  independent of  $h_{\mathcal{X}}$  such that

$$\|u^{n+1}(\mathcal{X}) - \mathcal{U}^{n+1}(\mathcal{X})\|_{\infty} \leq \lambda^* h_{\mathcal{X}}^2, \quad \forall n \geq 0.$$

*Proof.* Let  $\tilde{V}^{n+1}(\mathcal{X})$  be the unique exponential B-spline interpolant to the exact solution  $u^{n+1}(\mathcal{X})$  of the problem (8)-(9) given by

$$\tilde{V}^{n+1}(\mathcal{X}) = \sum_{m=-1}^{N_{\mathcal{X}}+1} \mathcal{B}_m^{n+1} \mathcal{Q}_m(\mathcal{X}). \quad (37)$$

At time level  $n + 1$ , we can write

$${}_0^C D_t^{\mu} \tilde{V}^{n+1}(\mathcal{X}) = \alpha \frac{\partial^2 \tilde{V}^{n+1}(\mathcal{X})}{\partial \mathcal{X}^2} + \beta \frac{\partial \tilde{V}^{n+1}(\mathcal{X})}{\partial x} - \gamma \tilde{V}^{n+1}(\mathcal{X}) + \tilde{\psi}^{n+1}(\mathcal{X}), \quad (-1 \leq n \leq N_t - 1) \quad (38)$$

with

$$\begin{cases} \tilde{V}^0(\mathcal{X}) = z(\mathcal{X}), \\ \tilde{V}^{n+1}(\mathcal{X}_0) = \mathcal{H}(t_{n+1}), & -1 \leq n \leq N_t - 1, \\ \tilde{V}^{n+1}(\mathcal{X}_{N_{\mathcal{X}}}) = \mathcal{G}(t_{n+1}), & -1 \leq n \leq N_t - 1. \end{cases} \quad (39)$$

Now using the equation (37) in (38) we have

$$\begin{aligned} \chi_1 \mathcal{B}_{m-1}^{n+1} + \chi_2 \mathcal{B}_m^{n+1} + \chi_3 \mathcal{B}_{m+1}^{n+1} &= \eta \mathcal{B}_{m-1}^n + \mathcal{B}_m^n + \eta \mathcal{B}_{m+1}^n - \sum_{k=1}^n w_k [(\eta \mathcal{B}_{m-1}^{n-k+1} + \mathcal{B}_m^{n-k+1} + \eta \mathcal{B}_{m+1}^{n-k+1}) \\ &\quad - (\eta \mathcal{B}_{m-1}^{n-k} + \mathcal{B}_m^{n-k} + \eta \mathcal{B}_{m+1}^{n-k})] + \tilde{\gamma} \tilde{\psi}^{n+1}(\mathcal{X}_m), \\ &\quad (0 \leq m \leq N_{\mathcal{X}}, -1 \leq n \leq N_t - 1) \end{aligned} \quad (40)$$

and also the boundary conditions in (39) together with (37) yield

$$\eta \mathcal{B}_{-1}^{n+1} = \mathcal{H}_{n+1} - \mathcal{B}_0^{n+1} - \eta \mathcal{B}_1^{n+1}, \quad (41)$$

$$\eta \mathcal{B}_{N_{\mathcal{X}}+1}^{n+1} = \mathcal{G}_{n+1} - \mathcal{B}_{N_{\mathcal{X}}}^{n+1} - \eta \mathcal{B}_{N_{\mathcal{X}}-1}^{n+1}. \quad (42)$$

Next, the subtraction of equation (23) from (40) gives

$$\begin{aligned} \chi_1 \lambda_{m-1}^{n+1} + \chi_2 \lambda_m^{n+1} + \chi_3 \lambda_{m+1}^{n+1} &= \eta \lambda_{m-1}^n + \lambda_m^n + \eta \lambda_{m+1}^n - \sum_{k=1}^n w_k [(\eta \lambda_{m-1}^{n-k+1} + \lambda_m^{n-k+1} + \eta \lambda_{m+1}^{n-k+1}) \\ &\quad - (\eta \lambda_{m-1}^{n-k} + \lambda_m^{n-k} + \eta \lambda_{m+1}^{n-k})] + \tilde{\gamma}(\tilde{\psi}_m^{n+1} - \psi_m^{n+1}), \\ &\quad (0 \leq m \leq N_\varkappa, -1 \leq n \leq N_t - 1). \end{aligned} \quad (43)$$

Also, subtracting equations (24) and (25) from (41) and (42) respectively yield

$$\eta \lambda_{-1}^{n+1} = -\lambda_0^{n+1} - \eta \lambda_1^{n+1}, \quad -1 \leq n \leq N_t - 1, \quad (44)$$

$$\eta \lambda_{N_\varkappa+1}^{n+1} = -\lambda_{N_\varkappa}^{n+1} - \eta \lambda_{N_\varkappa-1}^{n+1}, \quad -1 \leq n \leq N_t - 1, \quad (45)$$

where  $\lambda_m^{n+1} = \mathcal{B}_m^{n+1} - \mathcal{R}_m^{n+1}$  for  $-1 \leq m \leq N_\varkappa + 1$  and  $-1 \leq n \leq N_t - 1$ .

Now subtracting equation (13) from equation (38) and using Theorem 5.2 we have

$$\tilde{\psi}_m^{n+1} - \psi_m^{n+1} = O(h_\varkappa^2).$$

Thus, it follows from the above equation that

$$|\tilde{\psi}_m^{n+1} - \psi_m^{n+1}| \leq M h_\varkappa^2, \quad (46)$$

where  $M = \frac{c_0 h_\varkappa^2 \tilde{T}}{\Gamma(2-\mu)} + \alpha c_2 + \beta c_1 h_\varkappa + \gamma c_0 h_\varkappa^2$ .

Now, let us take  $\tilde{\lambda}^{n+1} = \max_{-1 \leq m \leq N_\varkappa+1} |\lambda_m^{n+1}|$ . Also, the initial condition of the problem implies that  $\tilde{\lambda}^0 = 0$ . At the first time level, i.e. for  $n = 0$ , the equation (43) can be written as

$$\chi_2 \lambda_m^1 = -\chi_1 \lambda_{m-1}^1 - \chi_3 \lambda_{m+1}^1 + \eta \lambda_{m-1}^0 + \lambda_m^0 + \eta \lambda_{m+1}^0 + \tilde{\gamma}(\tilde{\psi}_m^1 - \psi_m^1), \quad (47)$$

$$0 \leq m \leq N_\varkappa.$$

By using Taylor's series expansion, for sufficiently small  $h_\varkappa$ , we have

$$\chi_2 \lambda_m^1 = \lambda_m^1 (-\chi_1 - \chi_3) + \tilde{\gamma}(\tilde{\psi}_m^1 - \psi_m^1). \quad (48)$$

After rearranging the terms and taking the absolute values on both sides of equation (48) we have

$$|\lambda_m^1| = \left| \frac{\tilde{\gamma}(\tilde{\psi}_m^1 - \psi_m^1)}{(\chi_1 + \chi_2 + \chi_3)} \right| \leq \frac{\tilde{\gamma} M h_\varkappa^2}{(2\eta + 1)(1 + \gamma \tilde{\gamma})} \leq \tilde{M} h_\varkappa^2, \quad 0 \leq m \leq N_\varkappa, \quad (49)$$

where  $\tilde{M} = \frac{M \tilde{\gamma}}{(1+2\eta)(1+\gamma \tilde{\gamma})}$ . Also, from the boundary conditions we have the following esti-

mates for  $\lambda_{-1}^1$  and  $\lambda_{N_\varkappa+1}^1$  :

$$|\lambda_{-1}^1| \leq \tilde{k}h_\varkappa^2 \quad \text{and} \quad |\lambda_{N_\varkappa+1}^1| \leq \tilde{k}h_\varkappa^2, \quad (50)$$

where  $\tilde{k}$  is a constant independent of  $h_\varkappa$ .

Now combining the inequalities (49) and (50), we have

$$\tilde{\lambda}^1 \leq M_1 h_\varkappa^2, \quad (51)$$

where  $M_1 = \max\{\tilde{M}, \tilde{k}\}$ .

Next, we use the mathematical induction to prove that  $\tilde{\lambda}^{n+1} \leq r^* h_x^2$ , where  $r^*$  is a positive constant independent of  $h_x$ . Therefore, for this purpose we assume that

$$\tilde{\lambda}^j \leq K_j h_x^2 \quad (52)$$

is true for  $1 \leq j \leq n$ . Since in equation (51) we have shown that result (52) is true for  $j = 1$ . Now we will prove the result for  $j = n + 1$ . So, let  $\tilde{K} = \max_{0 \leq j \leq n} K_j$  and write the equation (43) in the form

$$\begin{aligned} \chi_2 \lambda_m^{n+1} = & -\chi_1 \lambda_{m-1}^{n+1} - \chi_3 \lambda_{m+1}^{n+1} + w_n (\eta \lambda_{m-1}^0 + \lambda_m^0 + \eta \lambda_{m+1}^0) + \sum_{k=0}^{n-1} (w_k - w_{k+1}) (\eta \lambda_{m-1}^{n-k} + \lambda_m^{n-k} + \eta \lambda_{m+1}^{n-k}) \\ & + \tilde{\gamma} (\tilde{\psi}_m^{n+1} - \psi_m^{n+1}), \\ & (0 \leq m \leq N_\varkappa). \end{aligned} \quad (53)$$

By applying Taylor's series expansion, for sufficiently small  $h_\varkappa$  we can have

$$\chi_2 \lambda_m^{n+1} = (-\chi_1 - \chi_3) \lambda_m^{n+1} + w_n (2\eta + 1) \lambda_m^0 + (2\eta + 1) \sum_{k=0}^{n-1} (w_k - w_{k+1}) \lambda_m^{n-k} + \tilde{\gamma} (\tilde{\psi}_m^{n+1} - \psi_m^{n+1}),$$

After rearranging the terms and taking the absolute values on both sides of above equation and using the assumption (52) we have

$$(\chi_1 + \chi_2 + \chi_3) |\lambda_m^{n+1}| \leq w_n (2\eta + 1) |\lambda_m^0| + (2\eta + 1) \sum_{k=0}^{n-1} (w_k - w_{k+1}) |\lambda_m^{n-k}| + \tilde{\gamma} |(\tilde{\psi}_m^{n+1} - \psi_m^{n+1})|$$

$$\leq \tilde{K} (2\eta + 1) \left( \sum_{k=0}^{n-1} \{(w_k - w_{k+1}) + w_n\} \right) h_\varkappa^2 + \tilde{\gamma} |(\tilde{\psi}_m^{n+1} - \psi_m^{n+1})|.$$

$$\text{Thus, } |\lambda_m^{n+1}| \leq \frac{w_0 \tilde{K} (2\eta + 1) h_\varkappa^2}{(\chi_1 + \chi_2 + \chi_3)} + \frac{\tilde{\gamma} |(\tilde{\psi}_m^{n+1} - \psi_m^{n+1})|}{(\chi_1 + \chi_2 + \chi_3)}.$$

Now using the inequality (46) we have

$$|\lambda_m^{n+1}| \leq \frac{\tilde{K}h_\varkappa^2}{(1+\gamma\tilde{\gamma})} + \frac{\tilde{\gamma}Mh_\varkappa^2}{(2\eta+1)(1+\gamma\tilde{\gamma})} \leq M^*h_\varkappa^2, \quad 0 \leq m \leq N_\varkappa, \quad (54)$$

where  $M^* = \frac{\tilde{K}}{(1+\gamma\tilde{\gamma})} + \frac{M\tilde{\gamma}}{(2\eta+1)(1+\gamma\tilde{\gamma})}$ .

Like before as in (50), we can obtain bounds for  $|\lambda_{-1}^{n+1}|$  and  $|\lambda_{N_\varkappa+1}^{n+1}|$ . With the help of these two bounds along with (54), it can be inferred that there exists a constant  $r^*$  independent of  $h_\varkappa$  such that

$$\tilde{\lambda}^{n+1} \leq r^*h_\varkappa^2, \quad (55)$$

where  $r^* = \max\{M^*, \tilde{k}\}$ .

Now

$$\tilde{V}^{n+1}(\varkappa) - \mathcal{U}^{n+1}(\varkappa) = \sum_{m=-1}^{N_\varkappa+1} (\mathcal{B}_m^{n+1} - \mathcal{R}_m^{n+1}) \mathcal{Q}_m(\varkappa).$$

Using Lemma 5.1 and inequality (55) in above relation we have

$$\|\tilde{V}^{n+1}(\varkappa) - \mathcal{U}^{n+1}(\varkappa)\|_\infty \leq \frac{5}{2}r^*h_\varkappa^2. \quad (56)$$

Using the triangle inequality we get

$$\|u^{n+1}(\varkappa) - \mathcal{U}^{n+1}(\varkappa)\|_\infty \leq \|u^{n+1}(\varkappa) - \tilde{V}^{n+1}(\varkappa)\|_\infty + \|\tilde{V}^{n+1}(\varkappa) - \mathcal{U}^{n+1}(\varkappa)\|_\infty. \quad (57)$$

Thus, using Theorem 5.2 and inequality (56), we get

$$\|u^{n+1}(\varkappa) - \mathcal{U}^{n+1}(\varkappa)\|_\infty \leq \lambda^*h_\varkappa^2, \quad \forall n \geq 0,$$

where  $\lambda^* = \frac{5}{2}r^* + c_0h_\varkappa^2$ .

Hence, the proof is complete.  $\square$

**Theorem 5.4.** *The present numerical scheme (23) for the TFBSM (8)-(9) is convergent of order  $O(h_t^{2-\mu} + h_\varkappa^2)$ .*

*Proof.* Theorem 5.3 together with relation (12) provides us the following result

$$\|u(\varkappa, t) - \mathcal{U}^{n+1}(\varkappa)\|_\infty \leq k_2h_t^{2-\mu} + k_3h_\varkappa^2,$$

where  $k_2$  and  $k_3$  are positive constants, and thus the proposed method is convergent of order  $O(h_t^{2-\mu} + h_\varkappa^2)$ .  $\square$

## 6. Numerical illustrations and applications

This section includes the numerical results for three test problems to examine the performance of the proposed numerical scheme. Furthermore, Example (6.4) is considered as



an application of the proposed scheme to price several different options like a European call option, European put option, and European double barrier knock-out call option. If  $u(\varkappa_m, t_n)$  and  $\mathcal{U}_m^n$  are the exact and approximate solutions of problem (8)-(9) respectively at the point  $(\varkappa_m, t_n)$ , then the accuracy of the numerical solution will be measured as follows

$$L_\infty(h_\varkappa, h_t) = \|u(\varkappa_m, t_n) - \mathcal{U}_m^n\|_\infty = \max_{1 \leq n \leq N_t} \max_{1 \leq m \leq N_\varkappa - 1} |u(\varkappa_m, t_n) - \mathcal{U}_m^n| \quad (58)$$

$$L_2(h_\varkappa, h_t) = \|u(\varkappa_m, t_n) - \mathcal{U}_m^n\|_2 = \max_{1 \leq n \leq N_t} \sqrt{h_\varkappa \sum_{m=1}^{N_\varkappa - 1} (u(\varkappa_m, t_n) - \mathcal{U}_m^n)^2} \quad (59)$$

The following formula is used to evaluate the order of convergence (EOC)

$$EOC = \begin{cases} \log_2 \left( \frac{L_j(h_\varkappa, (h_t)_1)}{L_j(h_\varkappa, (h_t)_2)} \right), & \text{in time,} \\ \log_2 \left( \frac{L_j((h_\varkappa)_1, h_t)}{L_j((h_\varkappa)_2, h_t)} \right), & \text{in space,} \end{cases} \quad (60)$$

where  $j = 2$  or  $\infty$ .

**Example 6.1.** [21] Let us consider the problem (8)-(9) on the domain  $(0, 1) \times (0, 1)$ ,

$${}_0^C D_t^\mu u(\varkappa, t) = \alpha \frac{\partial^2 u(\varkappa, t)}{\partial \varkappa^2} + \beta \frac{\partial u(\varkappa, t)}{\partial \varkappa} - \gamma u(\varkappa, t) + \psi(\varkappa, t),$$

with

$$\begin{cases} u(\varkappa, 0) = \varkappa^2(1 - \varkappa), \\ u(0, t) = 0, \\ u(1, t) = 0, \end{cases}$$

and the source term

$$\psi(\varkappa, t) = \frac{2}{\Gamma(3 - \mu)} t^{2-\mu} \varkappa^2(1 - \varkappa) + \frac{2}{\Gamma(2 - \mu)} t^{1-\mu} \varkappa^2(1 - \varkappa) - (t+1)^2 (\alpha(2-6\varkappa) + \beta\varkappa(2-3\varkappa) - \gamma\varkappa^2(1 - \varkappa)).$$

The exact solution of this test problem is  $u(\varkappa, t) = (t+1)^2 \varkappa^2(1 - \varkappa)$ . We will solve this problem with pre-mentioned values of parameters  $r_f = 0.05$ ,  $\sigma = 0.25$ .

Table 2 contains the errors  $L_2$  and  $L_\infty$  and respective orders of convergence, for Example 6.1 with  $\rho = 1.5$ ,  $\mu = 0.5$ ,  $h_\varkappa = 0.002$ , and different time spacings  $h_t$ . The results of this table validate the theoretical order of convergence proved in Theorem 5.4. Similarly,  $L_2$  and  $L_\infty$  errors with corresponding orders of convergence are calculated for  $\rho = 1.5$ ,  $N_t = 500$  and multiple values of  $\mu$ , and are shown in Tables 4 and 5, respectively. From these tables, it can be viewed that as we increase the discretization points  $N_\varkappa$ , the errors decrease and the numerically calculated spatial order of convergence is 2, which is in support of the result proved in Theorem 5.4.

Table 2: Errors  $L_2$  and  $L_\infty$  and corresponding orders of convergence with  $\mu = 0.5$ ,  $\rho = 1.5$  and  $h_{\mathcal{N}} = 0.002$  for Example 6.1

$h_t$	$\frac{1}{10}$	$\frac{1}{20}$	$\frac{1}{40}$	$\frac{1}{80}$	$\frac{1}{160}$	$\frac{1}{320}$
$L_2$	1.0584e-03	3.8720e-04	1.3997e-04	5.0197e-05	1.7890e-05	6.3288e-06
EOC	—	1.4507	1.4680	1.4794	1.4885	1.4991
$L_\infty$	1.5570e-03	5.6937e-04	2.0577e-04	7.3779e-05	2.6286e-05	9.2927e-06
EOC	—	1.4513	1.4684	1.4797	1.4889	1.5001

Table 3: Comparison of the maximum error  $L_\infty$  and the corresponding order of convergence with  $\mu = 0.7$ ,  $N_t = 1000$  and  $\rho = 1.5$  for Example 6.1.

$N_{\mathcal{N}}$	Present method		Method in [21]		Present method		Method in [21]	
	$L_\infty$ -error	EOC	$L_\infty$ -error	EOC	$L_2$ -error	EOC	$L_2$ -error	EOC
4	0.002	-	0.0030	-	0.001	-	0.0024	-
8	4.7739e-04	2.12	7.6750e-04	1.98	2.8144e-04	2.05	6.1678e-04	1.96
16	1.1112e-04	2.10	1.8629e-04	2.04	6.5497e-05	2.10	1.5079e-04	2.03
32	2.2337e-05	2.31	4.0698e-05	2.19	1.2680e-05	2.37	3.2995e-05	2.19

Table 4:  $L_2$  error and corresponding order of convergence for various of  $\mu$  with  $\rho = 1.5$  and  $N_t = 500$  for Example 6.1.

$\mu$	$N_{\mathcal{N}}$	$2^2$	$2^3$	$2^4$	$2^5$	$2^6$
0.2	$L_2$	1.3129e-03	3.2284e-04	7.9810e-05	1.9753e-05	4.7919e-06
	EOC	—	2.0239	2.0162	2.0145	2.0434
0.4	$L_2$	1.2590e-03	3.0844e-04	7.5439e-05	1.7916e-05	3.6469e-06
	EOC	—	2.0292	2.0316	2.0741	2.2965
0.6	$L_2$	1.1961e-03	2.8875e-04	6.6856e-05	1.2634e-05	2.6656e-06
	EOC	—	2.0504	2.1107	2.4038	2.2448

Table 5: Maximum error  $L_\infty$  and corresponding order of convergence for various  $\mu$  with  $\rho = 1.5$  and  $N_t = 500$  for Example 6.1.

$\mu$	$N_{\mathcal{N}}$	$2^2$	$2^3$	$2^4$	$2^5$	$2^6$
0.2	$L_\infty$	2.3031e-03	5.4273e-04	1.3376e-04	3.3122e-05	8.0812e-06
	EOC	—	2.0852	2.0206	2.0137	2.0352
0.4	$L_\infty$	2.2197e-03	5.2005e-04	1.2692e-04	3.0408e-05	6.3578e-06
	EOC	—	2.0936	2.0348	2.0614	2.2579
0.6	$L_\infty$	2.1229e-03	4.8913e-04	1.1338e-04	2.2242e-05	5.2007e-06
	EOC	—	2.1177	2.1090	2.3499	2.0965

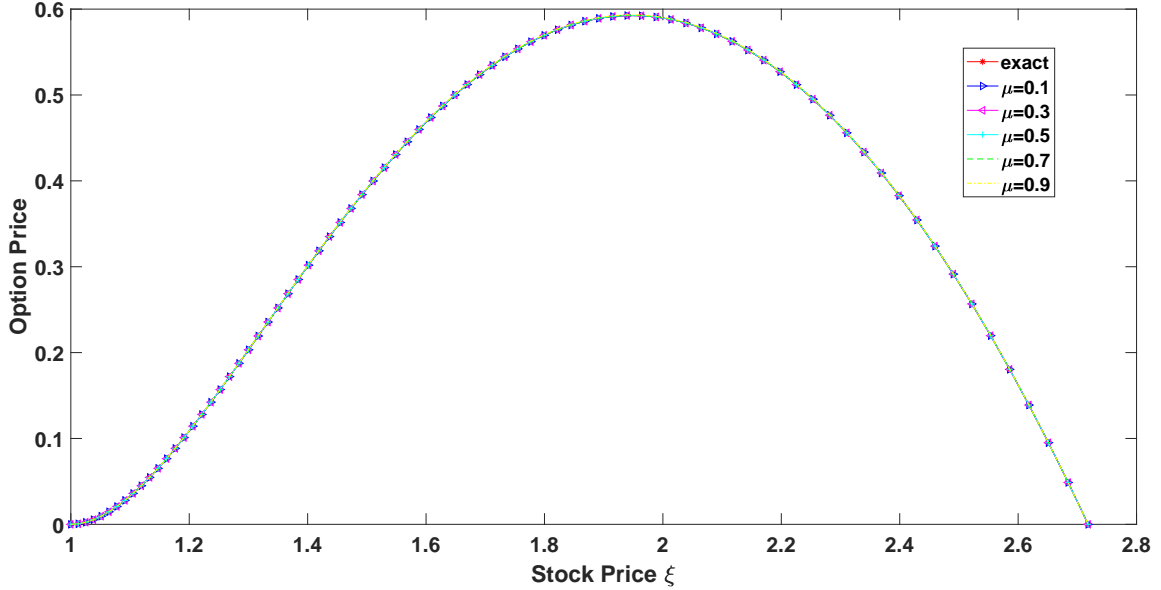


Figure 1: Exact and numerical solutions of Example 6.1 with  $\rho = 1.5$  and  $N_x = N_t = 80$ .

Figures 1, 4, and 6 represent the exact and numerical solutions taking different fractional orders  $\mu$  for Examples 6.1, 6.2, and 6.3 respectively. From these graphs, we can say that the proposed method approximates the TFBSM very well. The graphs shown in Figures 2, 5, and 7 compare the numerical and exact solutions of Examples 6.1, 6.2, and 6.3 respectively, at different time levels. From these graphs, we observe that the numerical and exact solutions follow almost the same path. Further, Figure 3 shows the three-dimensional plots of the maximum errors for Example 6.1 with  $\rho = 1.5$ ,  $\mu = 0.9$ , and different  $N_x$ ,  $N_t$ . Moreover, for  $\rho = 8.6$ ,  $\mu = 0.99$ , and different  $N_x$ ,  $N_t$  the three-dimensional graphics of the maximum errors for Example 6.3 are given in Figure 8 and show that the errors decrease as the discretization points  $N_x$  and  $N_t$  increase.

**Example 6.2.** Let us consider the problem (8)-(9) on the domain  $(0, 1) \times (0, 1)$ ,

$${}_0^C D_t^\mu u(x, t) = \alpha \frac{\partial^2 u(x, t)}{\partial x^2} + \beta \frac{\partial u(x, t)}{\partial x} - \gamma u(x, t) + \psi(x, t),$$

with

$$\begin{cases} u(x, 0) = 1 + x^2 + x^3, \\ u(0, t) = (1 + t)^2, \\ u(1, t) = 3(1 + t)^2, \end{cases}$$

and the source term

$$\psi(x, t) = \left( \frac{2t^{2-\mu}}{\Gamma(3-\mu)} + \frac{2t^{1-\mu}}{\Gamma(2-\mu)} \right) (1+x^2+x^3) - (t+1)^2 (\alpha(6x+2) + \beta x(2+3x) - \gamma(1+x^2+x^3)).$$

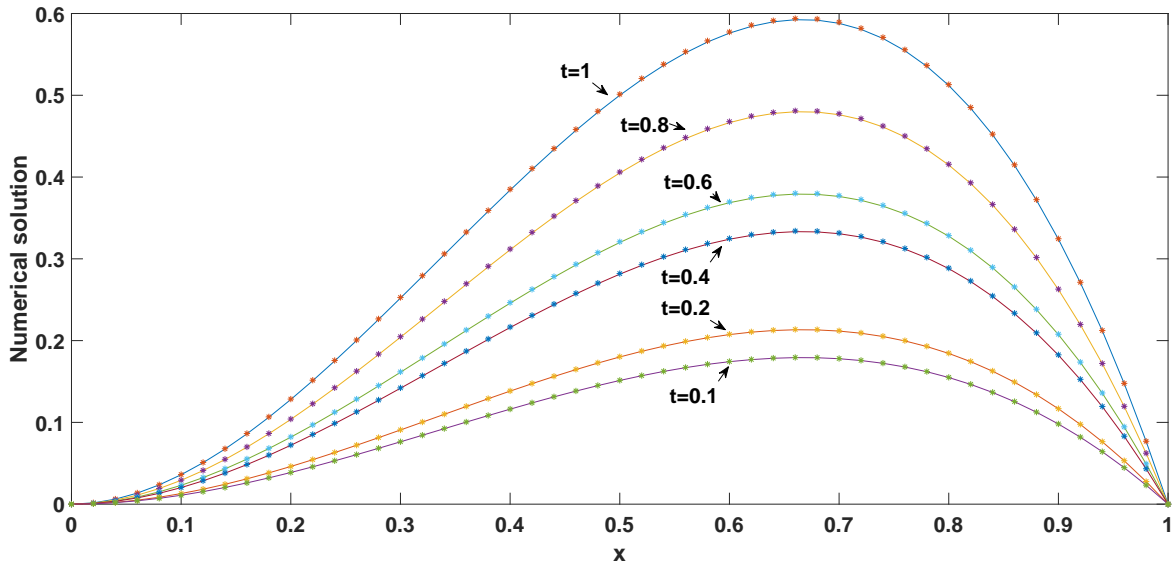
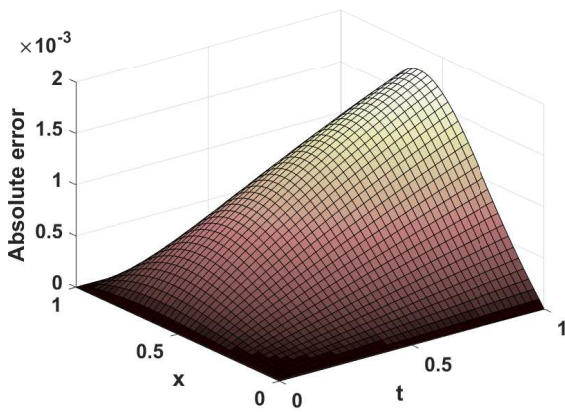
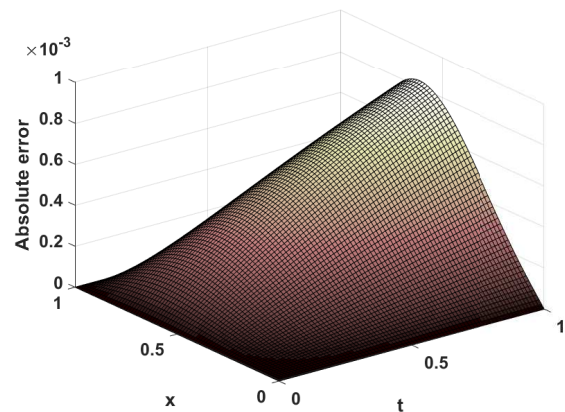


Figure 2: Numerical solution (starred line) and exact solution (solid line) of Example 6.1 with  $\mu = 0.9$ ,  $\rho = 1.5$  and  $N_x = N_t = 50$ , at different time levels.



(a)  $N_x = N_t = 40$



(b)  $N_x = N_t = 80$

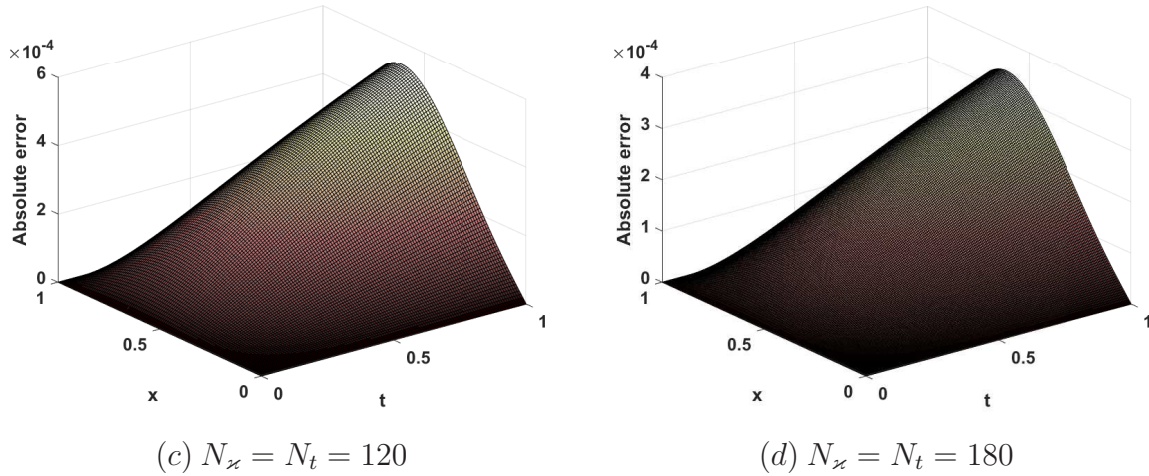


Figure 3: Maximum absolute error plots for different mesh sizes for Example 6.1 with  $\mu = 0.9$  and  $\rho = 1.5$ .

Table 6:  $L_2$  error and corresponding order of convergence for various  $\mu$  with  $\rho = 0.5$  and  $N_t = 2500$  for Example 6.2.

$\mu$	$N_x$	$2^2$	$2^3$	$2^4$	$2^5$	$2^6$
0.2	$L_2$	2.0482e-03	5.1071e-04	1.2755e-04	3.1892e-05	7.9881e-06
	EOC	—	2.0037	2.0015	1.9998	1.9973
0.4	$L_2$	2.0425e-03	5.0936e-04	1.2732e-04	3.1946e-05	8.1137e-06
	EOC	—	2.0036	2.0003	1.9947	1.9772
0.6	$L_2$	2.0413e-03	5.0980e-04	1.2819e-04	3.2936e-05	9.1312e-06
	EOC	—	2.0015	1.9916	1.9606	1.8508

The exact solution of this test problem is  $u(x, t) = (t + 1)^2(1 + x^2 + x^3)$ . We will solve this problem with pre-mentioned values of parameters  $r_f = 0.5$ ,  $\alpha = 1$ .

The numerical results obtained by applying the proposed method for Example 6.2 are given in Tables 6, 7, 8, and 9. Tables 6 and 7, give the errors  $L_2$  and  $L_\infty$  with the corresponding orders of convergence calculated for  $\rho = 0.5$ ,  $N_t = 2500$ , and different fractional orders  $\mu$ . From these tables, we can see that the numerically evaluated spatial order of convergence comes out to be two. Similarly, from Tables 9 and 10, we can see that the errors  $L_2$  and  $L_\infty$  decrease as we increase the discretization points  $N_x$ . Also, these tables show that the temporal order of convergence is  $O(h_t^{2-\mu})$ , which is consistent with Theorem 5.4.

**Example 6.3.** Let us consider the problem (1)-(3) on the domain  $(0, 1) \times (0, 1)$ ,

$${}^C D_t^\mu u(x, t) = \alpha \frac{\partial^2 u(x, t)}{\partial x^2} + \beta \frac{\partial u(x, t)}{\partial x} - \gamma u(x, t) + \psi(x, t),$$

Table 7: Maximum absolute error  $L_\infty$  and corresponding order of convergence for various  $\mu$  with  $\rho = 0.5$  and  $N_t = 2500$  for Example 6.2.

$\mu$	$N_\varkappa$	$2^2$	$2^3$	$2^4$	$2^5$	$2^6$
0.2	$L_\infty$	2.7740e-03	6.9807e-04	1.7615e-04	4.4043e-05	1.1038e-05
	EOC	–	1.9905	1.9866	1.9998	1.9965
0.4	$L_\infty$	2.7661e-03	6.9623e-04	1.7582e-04	4.4114e-05	1.1209e-05
	EOC	–	1.9902	1.9855	1.9948	1.9765
0.6	$L_\infty$	2.7643e-03	6.9683e-04	1.7701e-04	4.5467e-05	1.2603e-05
	EOC	–	1.9880	1.9770	1.9610	1.8510

Table 8:  $L_2$  and  $L_\infty$  errors and corresponding orders of convergence with  $\mu = 0.3$ ,  $\rho = 0.5$  and  $N_\varkappa = 1000$  for Example 6.2.

$N_t$	10	20	40	80	160	320
$L_2$	6.1294e-04	1.9775e-04	6.3151e-05	2.0026e-05	6.3280e-06	2.0061e-06
EOC	–	1.6321	1.6468	1.6570	1.6620	1.6574
$L_\infty$	8.3939e-04	2.7082e-04	8.6487e-05	2.7426e-05	8.6669e-06	2.7478e-06
EOC	–	1.6320	1.6468	1.6569	1.6620	1.6572

Table 9:  $L_2$  and  $L_\infty$  errors and corresponding orders of convergence with  $\mu = 0.7$ ,  $\rho = 0.5$  and  $N_\varkappa = 1000$  for Example 6.2.

$N_t$	10	20	40	80	160	320
$L_2$	3.9975e-03	1.6365e-03	6.6783e-04	2.7203e-04	1.1069e-04	4.5023e-05
EOC	–	1.2885	1.2931	1.2957	1.2972	1.2978
$L_\infty$	5.4792e-03	2.2432e-03	9.1541e-04	3.7288e-04	1.5173e-04	6.1715e-05
EOC	–	1.2884	1.2931	1.2957	1.2972	1.2978

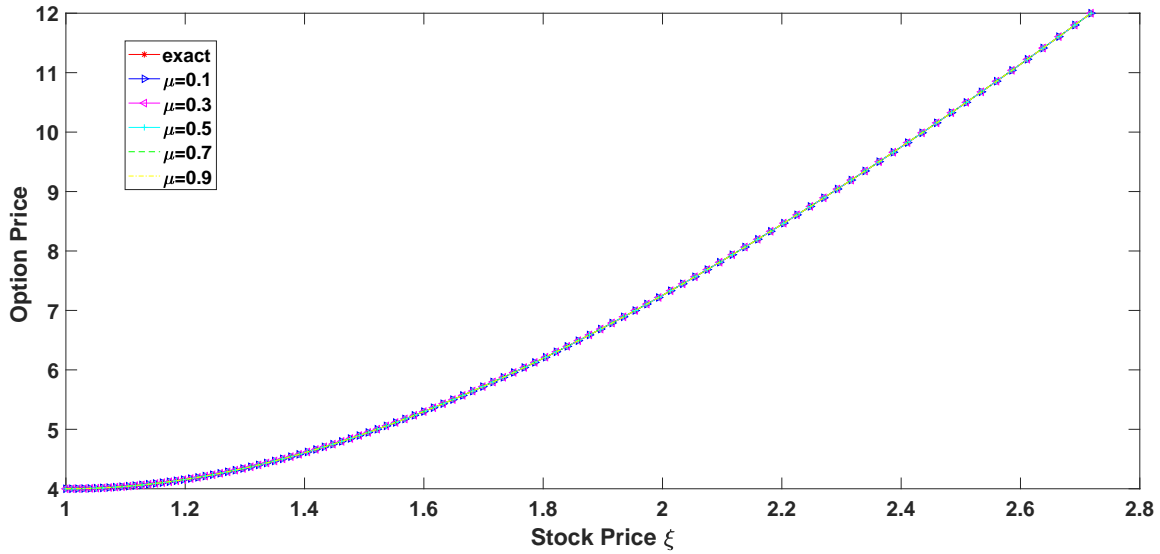


Figure 4: The exact and numerical solutions of Example 6.2 with  $\rho = 0.5$  and  $N_x = N_t = 100$ .

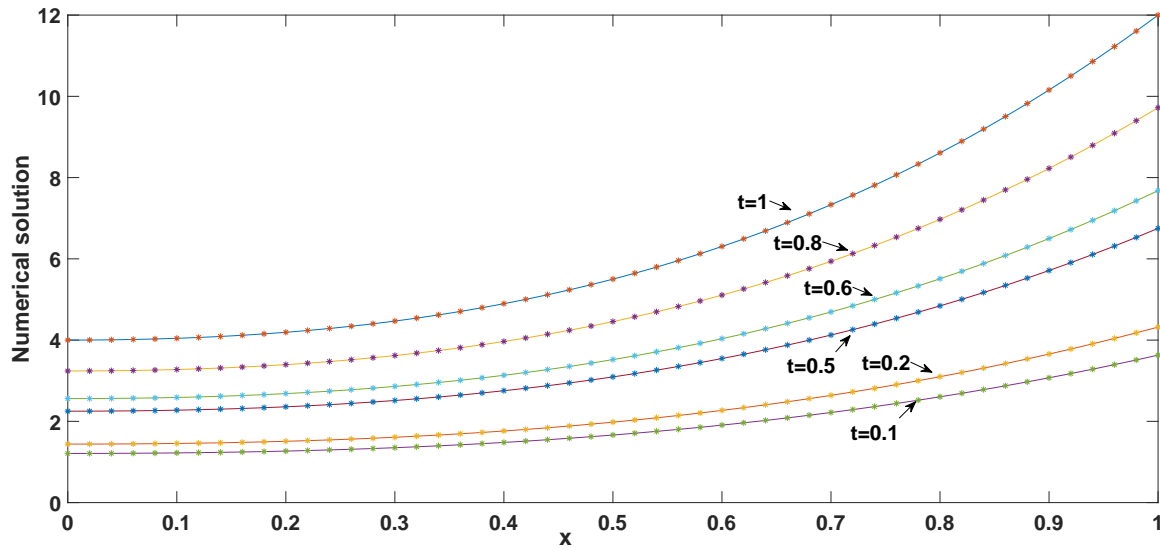


Figure 5: The numerical solution (starred line) and the exact solution (solid line) of Example 6.2 with  $\mu = 0.9$ ,  $\rho = 0.5$  and  $N_x = N_t = 50$ , at different time  $t$ .

Table 10:  $L_2$  and  $L_\infty$  errors and corresponding orders of convergence with  $\mu = 0.5$ ,  $\rho = 8.6$  and  $N_\varkappa = 1500$  for Example 6.3.

$N_t$	$2^3$	$2^4$	$2^5$	$2^6$	$2^7$	$2^8$
$L_2$	3.8050e-04	1.4288e-04	5.2529e-05	1.9074e-05	6.8818e-06	2.4842e-06
EOC	–	1.4131	1.4436	1.4615	1.4708	1.4700
$L_\infty$	5.7987e-04	2.1766e-04	7.9979e-05	2.9009e-05	1.0437e-05	3.7441e-06
EOC	–	1.4137	1.4444	1.4631	1.4747	1.4790

Table 11:  $L_2$  and  $L_\infty$  errors and corresponding orders of convergence with  $\mu = 0.9$ ,  $\rho = 8.6$  and  $N_\varkappa = 1000$  for Example 6.3.

$N_t$	$2^3$	$2^4$	$2^5$	$2^6$	$2^7$	$2^8$
$L_2$	1.7975e-03	8.6241e-04	4.0834e-04	1.9201e-04	8.9977e-05	4.2101e-05
EOC	–	1.0595	1.0786	1.0886	1.0936	1.0957
$L_\infty$	2.7482e-03	1.3184e-03	6.2410e-04	2.9340e-04	1.3742e-04	6.4243e-05
EOC	–	1.0597	1.0789	1.0889	1.0942	1.0970

with

$$\begin{cases} u(\varkappa, 0) = \varkappa^4(\varkappa - 1), \\ u(0, t) = 0, \\ u(1, t) = 0, \end{cases}$$

and the source term

$$\psi(\varkappa, t) = \frac{6}{\Gamma(4 - \mu)} t^{3-\mu} (\varkappa^5 - \varkappa^4) - (t^3 + 1)(4\alpha \varkappa^2(5\varkappa - 3) + \beta \varkappa^3(5\varkappa - 4) - \gamma \varkappa^4(\varkappa - 1)).$$

The exact solution of this test problem is  $u(\varkappa, t) = (t^3 + 1)\varkappa^4(\varkappa - 1)$ . We will solve this problem with pre-mentioned values of parameters  $r_f = 0.02$ ,  $\sigma = 0.8$ .

Tables 10 and 11 display  $L_2$  and  $L_\infty$  errors with the respective orders of convergence for Example 6.3 that have been evaluated for the time fractional-orders  $\mu = 0.5$  and  $\mu = 0.9$ , respectively. One can see that the orders of convergence shown in Tables 10 and 11 are sufficiently close to 1.5 and 1.1 respectively. So from here, we conclude that the numerically evaluated temporal order of convergence is  $O(h_t^{2-\mu})$  which is consistent with Theorem 5.4. In a similar manner, the errors  $L_2$  and  $L_\infty$  with the respective spatial orders of convergence are tabulated in Tables 12 and 13 respectively.

**Example 6.4.** Let us consider the TFBSM [45]

$$\frac{\partial^\mu \mathcal{V}(\xi, \tau)}{\partial \tau^\mu} + \frac{\sigma^2 \xi^2}{2} \frac{\partial^2 \mathcal{V}(\xi, \tau)}{\partial \xi^2} + (r_f - D_Y) \xi \frac{\partial \mathcal{V}(\xi, \tau)}{\partial \xi} - r_f \mathcal{V}(\xi, \tau) = 0, \quad (\xi, \tau) \in (\xi_{I_p}, \xi_{F_p}) \times (0, \tilde{T}), \quad (61)$$



Table 12:  $L_2$  error and corresponding order of convergence for various  $\mu$  with  $\rho = 7.4$  and  $N_t = 1000$  for Example 6.3.

$\mu$	$N_x$	$2^3$	$2^4$	$2^5$	$2^6$	$2^7$
0.2	$L_2$	3.6198e-03	9.8464e-04	2.5136e-04	6.3176e-05	1.5823e-05
	EOC	—	1.8782	1.9699	1.9923	1.9973
0.4	$L_2$	3.5812e-03	9.7332e-04	2.4846e-04	6.2494e-05	1.5704e-05
	EOC	—	1.8794	1.9699	1.9912	1.9926
0.6	$L_2$	3.5451e-03	9.6305e-04	2.4606e-04	6.2173e-05	1.5916e-05
	EOC	—	1.8801	1.9686	1.9847	1.9658

Table 13: Maximum absolute error  $L_\infty$  and corresponding order of convergence for various  $\mu$  with  $\rho = 8.6$  and  $N_t = 1000$  for Example 6.3.

$\mu$	$N_x$	$2^3$	$2^4$	$2^5$	$2^6$	$2^7$
0.2	$L_\infty$	5.9815e-03	1.5523e-03	4.0375e-04	1.0171e-04	2.5489e-05
	EOC	—	1.9461	1.9429	1.9890	1.9965
0.4	$L_\infty$	5.9791e-03	1.5404e-03	3.9964e-04	1.0075e-04	2.5332e-05
	EOC	—	1.9566	1.9465	1.9879	1.991
0.6	$L_\infty$	5.9723e-03	1.5384e-03	3.9623e-04	1.0035e-04	2.5693e-05
	EOC	—	1.9569	1.9570	1.9813	1.9656

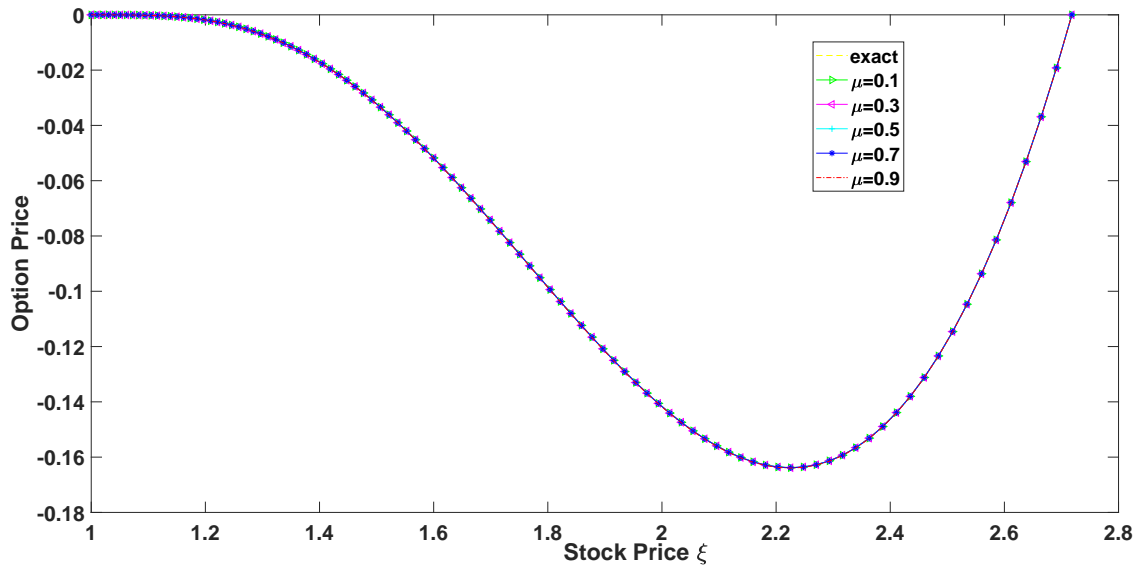


Figure 6: The exact and numerical solutions of Example 6.3 with  $\rho = 8.6$  and  $N_x = N_t = 100$ .

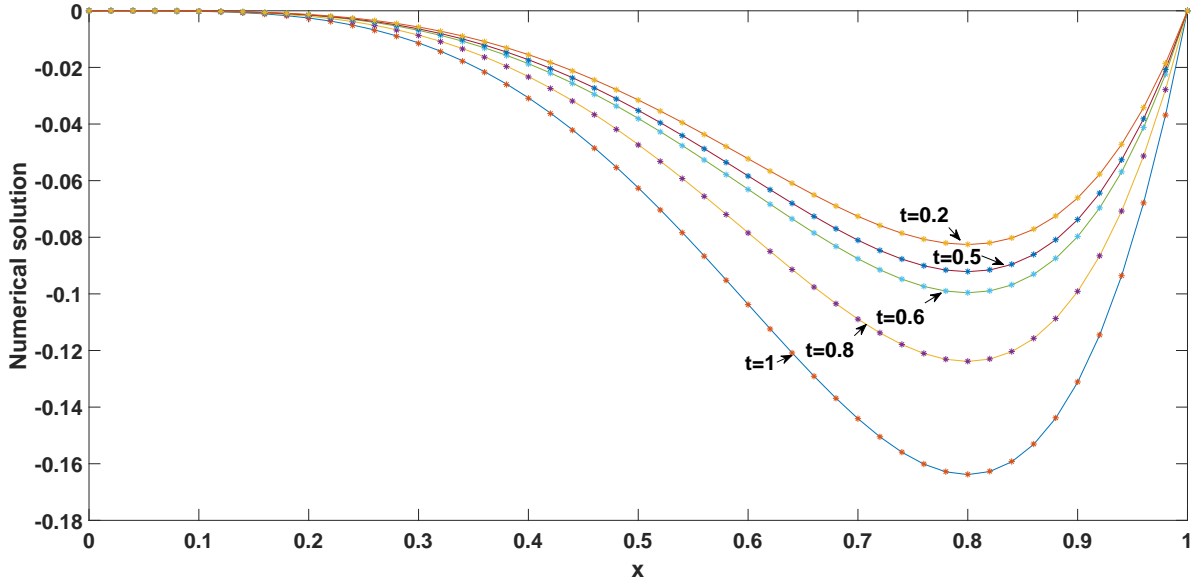
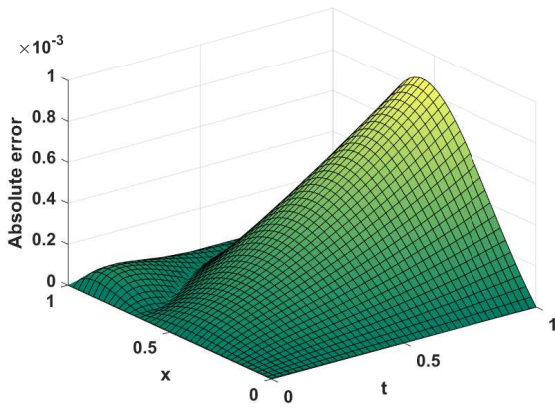
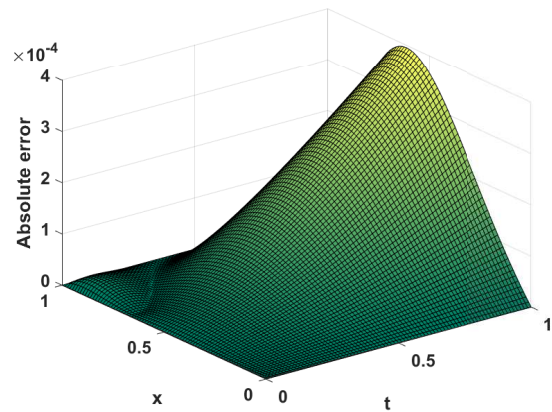


Figure 7: The numerical solution (starred line) and exact the solution (solid line) of Example 6.3 with  $\mu = 0.5$ ,  $\rho = 8.6$  and  $N_x = N_t = 50$  at different time  $t$ .



(a)  $N_x = N_t = 40$



(b)  $N_x = N_t = 80$

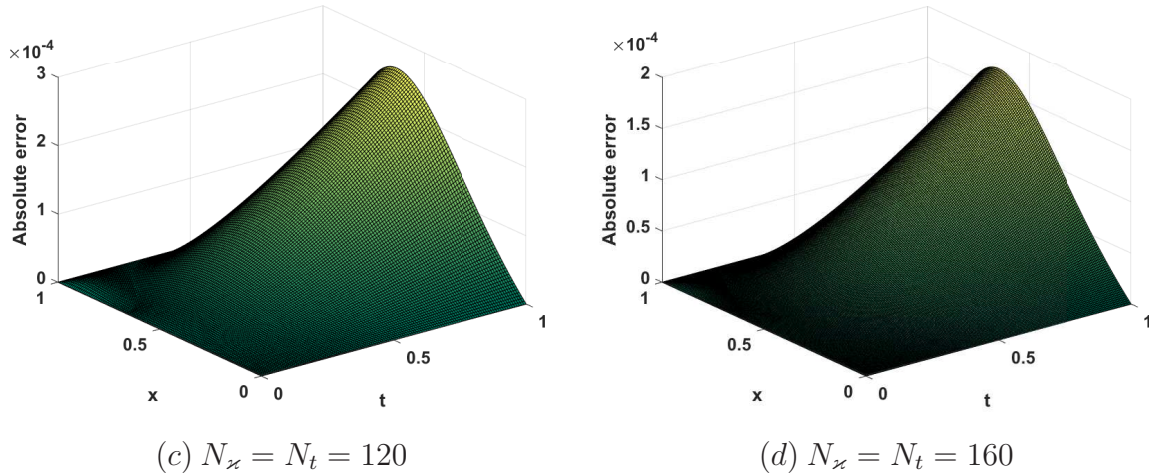


Figure 8: Maximum absolute error plots for different mesh sizes for Example 6.3 with  $\mu = 0.99$  and  $\rho = 8.6$ .

$$\begin{cases} \mathcal{V}(\xi, \tilde{T}) = \phi(\xi), \\ \mathcal{V}(\xi_{I_p}, \tau) = \mathcal{H}(\tau), \\ \mathcal{V}(\xi_{F_p}, \tau) = \mathcal{G}(\tau), \end{cases}$$

The above model describes different option values depending on the functions  $\phi(\xi)$ ,  $\mathcal{H}(\tau)$ , and  $\mathcal{G}(\tau)$ .

- If  $\phi(\xi) = \max\{\tilde{K} - \xi, 0\}$ ,  $\mathcal{H}(\tau) = \tilde{K}e^{-r_f(\tilde{T}-\tau)}$  and  $\mathcal{G}(\tau) = D_Y = 0$ , then the model represents the European put option.
- If  $\phi(\xi) = \max\{\xi - \tilde{K}, 0\}$ ,  $\mathcal{H}(\tau) = D_Y = 0$  and  $\mathcal{G}(\tau) = \xi_{I_f} - \tilde{K}e^{-r_f(\tilde{T}-\tau)}$ , then the model represents the European call option.
- And if  $\phi(\xi) = \max\{\xi - \tilde{K}, 0\}$  and  $\mathcal{H}(\tau) = \mathcal{G}(\tau) = 0$ , then the model describes the European double barrier knock-out call option.

For solving European call and European put option models numerically we have taken the parameters  $\sigma = 0.55$ ,  $r_f = 0.05$ ,  $\xi_{I_p} = 0.1(I_p = -2.3)$ ,  $\xi_{F_p} = 100(F_p = 4.6)$ ,  $\tilde{T} = 1$ (year), and the strike price  $\tilde{K} = 50$ . Also, we take the parameters  $\sigma = 0.55$ ,  $r_f = 0.03$ ,  $\xi_{I_p} = 3(I_p = 1.1)$ ,  $\xi_{F_p} = 15(F_p = 2.7)$ ,  $\tilde{T} = 1$ (year), the dividend yield  $D_Y = 0.01$ , and the strike price  $\tilde{K} = 10$ , to study the European double barrier knock-out call option model numerically.

Figures 9 and 10 show how the orders of fractional derivative affect the European call option and put option, respectively. From these two figures, we can observe that when the stock price  $\xi$  is less or greater than the strike price  $\tilde{K}$ , the option price is slightly affected by the order of the time-fractional derivative. And when the stock price  $\xi$  is close to the strike price  $\tilde{K}$ , the option price is significantly affected by the time-fractional derivative order. Further, Figure 11 show how the different parameters affect the European put

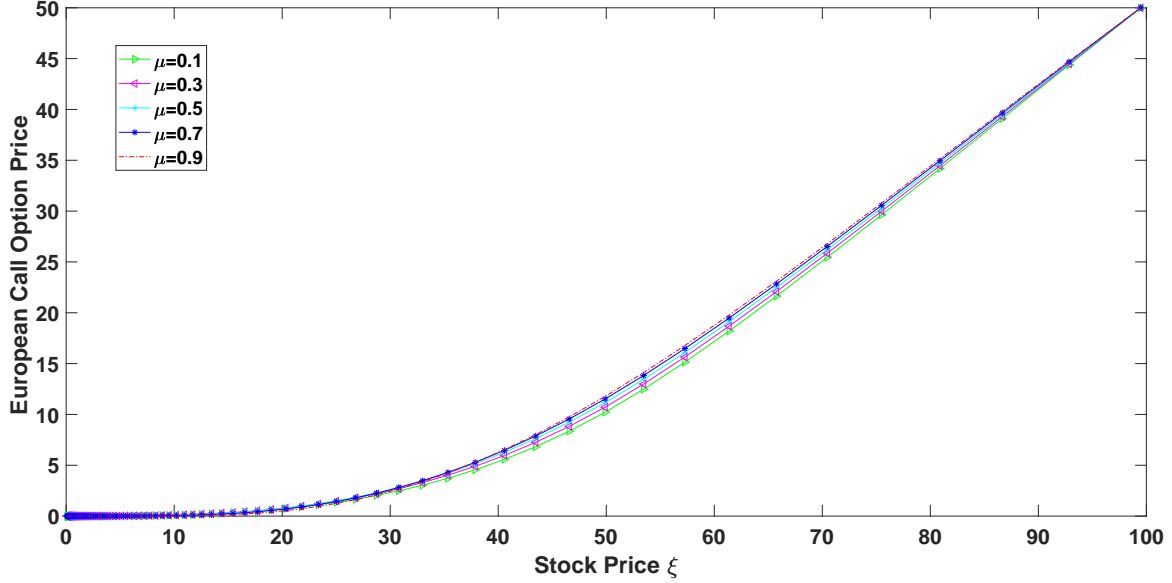


Figure 9: European call option curves with  $\rho = 1.5$ ,  $N_z = N_t = 100$  and different  $\mu$  for Example 6.4.

option price governed by TFBSM. From Figure 11(a), it can be observed that the rate of interest and the options are inversely proportional, i.e the higher the rate of interest, the lower the option. Similarly, Figure 11(b) reflects, how the stock price volatility influences the option price and supports a well-known statement “The higher the risk, the higher the return”. In Figure 12, the graph is plotted between the stock price  $\xi$  and the double barrier option price  $\mathcal{V}$  for various values of time-fractional order  $\mu$ . It is worth noting here that for  $\mu = 1$ , the TFBSM converts to the classical Black-Scholes model. This Figure 12 depicts that the double barrier option price is highly influenced by the time-fractional order. More specifically, the option price is inversely proportional to the fractional-order when the stock price is greater than or near the strike price  $\tilde{K}$ . And the peak of the option price curve occurred corresponding to  $\mu = 0.2$ . This tells us that TFBSM can explain the jump movement of the problem much more clearly than the classic Black-Scholes model.

## 7. Conclusion

In this paper, an efficient collocation method based on exponential B-spline functions is introduced to solve the TFBSM governing European options. First, we have changed the modified R-L fractional derivative operator to the Caputo fractional derivative operator by applying the variable transformation, then used the exponential B-spline functions to discretize the space derivative and a finite difference method to discretize the Caputo fractional derivative. As a result of the use of the exponential B-spline collocation method, a tri-diagonal algebraic system has been obtained that can be solved by the Thomas algorithm. Furthermore, the proposed numerical scheme has been shown to be unconditionally stable via the von-Neumann method. The method is implemented on a number of

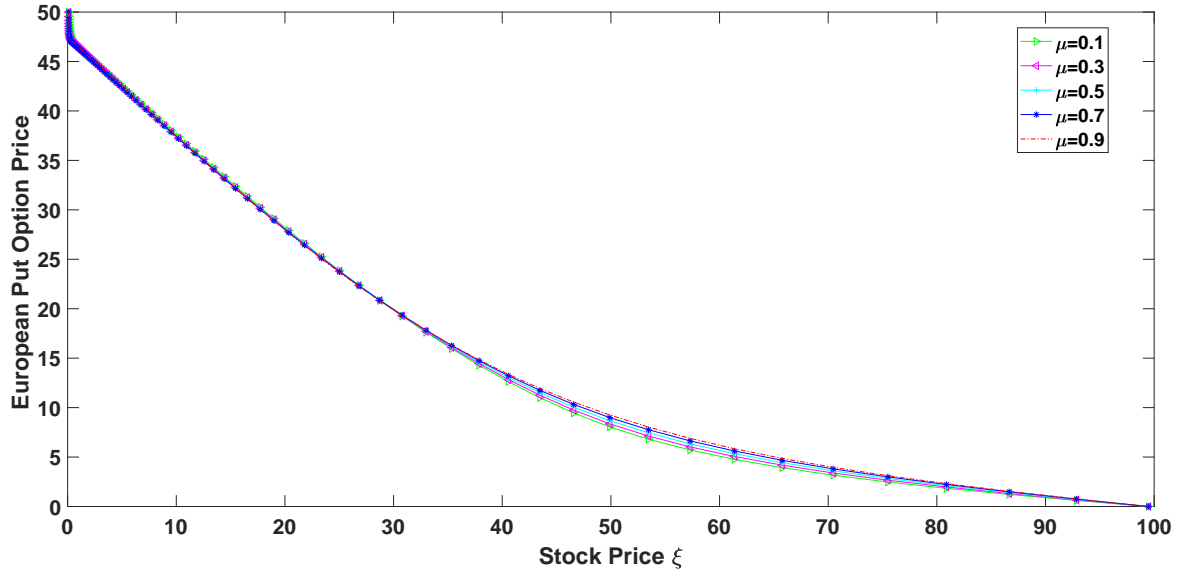


Figure 10: European put option curves with  $\rho = 1.5$ ,  $N_x = N_t = 100$  and different  $\mu$  for Example 6.4.

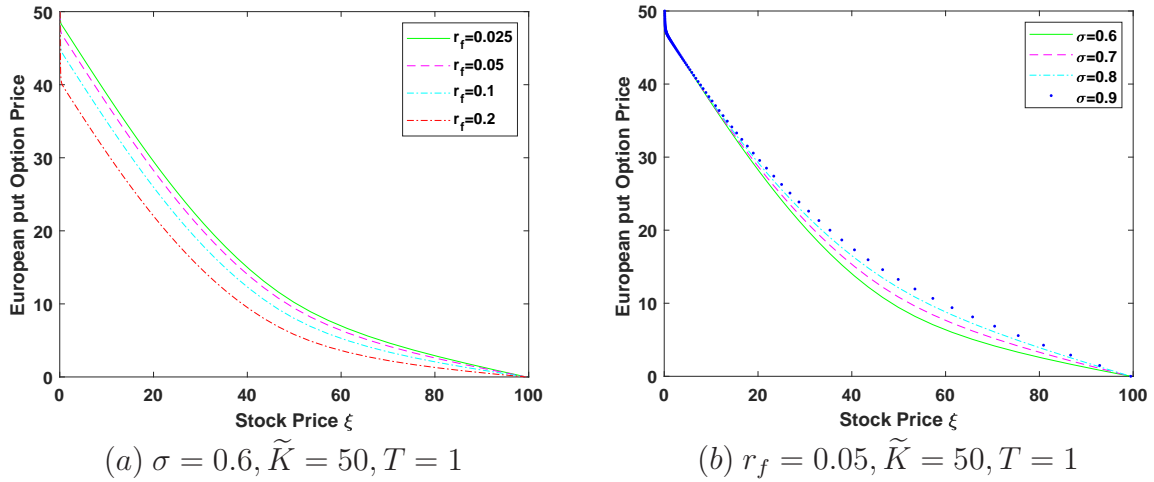


Figure 11: European put option curves with different values of parameters for Example 6.4.

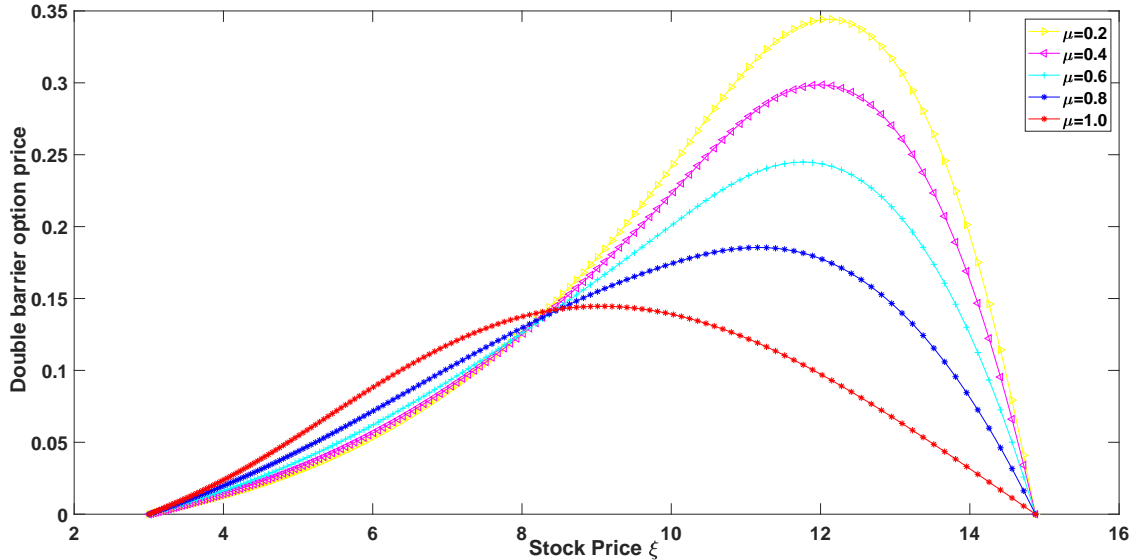


Figure 12: Double barrier option curves with  $\rho = 1.5$ ,  $N_x = N_t = 150$  and different  $\mu$  for Example 6.4.

numerical examples. And the obtained results confirm that the method is capable of approximating the TFBSM. In addition, as an application, the numerical scheme proposed for the TFBSM has been used to price several different European options and it has been observed that the order of the time-fractional derivative has a great impact on the option prices. Since the proposed scheme works well for the TFBSM, so it is our intention to extend this idea to solve other fractional problems numerically.

## Declarations

**Conflict of interest:** The authors declare that they have no known competing financial interests or personal relationships that could have appeared to influence the work reported in this paper.

## References

- [1] F. Black, M. Scholes, The pricing of options and corporate liabilities, in: World Scientific Reference on Contingent Claims Analysis in Corporate Finance: Volume 1: Foundations of CCA and Equity Valuation, World Scientific, 2019, pp. 3–21.
- [2] R. C. Merton, Theory of rational option pricing, The Bell Journal of economics and management science (1973) 141–183.
- [3] M. R. Rodrigo, R. S. Mamon, An alternative approach to solving the Black-Scholes equation with time-varying parameters, Applied Mathematics Letters 19 (4) (2006) 398–402.

- [4] M. Bohner, Y. Zheng, On analytical solutions of the Black–Scholes equation, *Applied Mathematics Letters* 22 (3) (2009) 309–313.
- [5] P. Amster, C. Averbuj, M. Mariani, Solutions to a stationary nonlinear Black–Scholes type equation, *Journal of Mathematical Analysis and Applications* 276 (1) (2002) 231–238.
- [6] P. Amster, C. Averbuj, M. Mariani, Stationary solutions for two nonlinear Black–Scholes type equations, *Applied Numerical Mathematics* 47 (3-4) (2003) 275–280.
- [7] R. Company, E. Navarro, J. R. Pintos, E. Ponsoda, Numerical solution of linear and nonlinear black–scholes option pricing equations, *Computers & Mathematics with Applications* 56 (3) (2008) 813–821.
- [8] R. Company, L. Jódar, J. R. Pintos, A numerical method for European Option Pricing with transaction costs nonlinear equation, *Mathematical and computer modelling* 50 (5-6) (2009) 910–920.
- [9] Z. Cen, A. Le, A robust and accurate finite difference method for a generalized Black–Scholes equation, *Journal of Computational and Applied Mathematics* 235 (13) (2011) 3728–3733.
- [10] P. Carr, L. Wu, The finite moment log stable process and option pricing, *The Journal of Finance* 58 (2) (2003) 753–777.
- [11] Wyss, Walter, The fractional Black-Scholes equation, *Fractional Calculus and Applied Analysis* 1 (2000) 51–61.
- [12] A. Carlea, D. Del-Castillo-Negrete, Fractional diffusion models of option prices in markets with jumps, *Physica A: Statistical Mechanics and its Applications* 374 (2) (2007) 749–763.
- [13] G. Jumarie, Stock exchange fractional dynamics defined as fractional exponential growth driven by (usual) Gaussian white noise. Application to fractional Black–Scholes equations, *Insurance: Mathematics and Economics* 42 (1) (2008) 271–287.
- [14] G. Jumarie, Derivation and solutions of some fractional Black–Scholes equations in coarse-grained space and time. Application to Merton’s optimal portfolio, *Computers & Mathematics with Applications* 59 (3) (2010) 1142–1164.
- [15] J. R. Liang, J. Wang, W. J. Zhang, W. Y. Qiu, F. Y. Ren, Option pricing of a bi-fractional Black–Merton–Scholes model with the Hurst exponent  $H$  in  $[1/2, 1]$ , *Applied Mathematics Letters* 23 (8) (2010) 859–863.
- [16] W. Chen, X. Xu, S.-P. Zhu, Analytically pricing double barrier options based on a time-fractional Black–Scholes equation, *Computers & Mathematics with Applications* 69 (12) (2015) 1407–1419.

- [17] D. Prathumwan, K. Trachoo, On the solution of two-dimensional fractional Black–Scholes equation for European put option, *Advances in Difference Equations* 2020 (1) (2020) 1–9.
- [18] M. Ghandehari, M. Ranjbar, European option pricing of fractional version of the Black-Scholes model: Approach via expansion in series, *International Journal of Nonlinear Science* 17 (2) (2014) 105–110.
- [19] S. O. Edeki, O. O. Ugbebor, E. A. Owoloko, Analytical solution of the time-fractional order Black-Scholes model for stock option valuation on no dividend yield basis, *IAENG International Journal of Applied Mathematics* 47 (4) (2017) 1–10.
- [20] A. N. Fall, S. N. Ndiaye, N. Sene, Black–Scholes option pricing equations described by the Caputo generalized fractional derivative, *Chaos, Solitons & Fractals* 125 (2019) 108–118.
- [21] H. Zhang, F. Liu, I. Turner, Q. Yang, Numerical solution of the time-fractional Black–Scholes model governing European options, *Computers & Mathematics with Applications* 71 (9) (2016) 1772–1783.
- [22] R. H. De Staelen, A. S. Hendy, Numerically pricing double barrier options in a time-fractional Black–Scholes model, *Computers & Mathematics with Applications* 74 (6) (2017) 1166–1175.
- [23] L. Song, W. Wang, Solution of the fractional Black-Scholes option pricing model by finite difference method, *Abstract and Applied Analysis* 2013 (2013).
- [24] M. N. Koleva, L. G. Vulkov, Numerical solution of time-fractional Black–Scholes equation, *Computational and Applied Mathematics* 36 (4) (2017) 1699–1715.
- [25] A. Golbabai, E. Mohebianfar, A new stable local radial basis function approach for option pricing, *Computational Economics* 49 (2) (2017) 271–288.
- [26] G. Hariharan, S. Padma, P. Pirabaharan, An efficient wavelet based approximation method to time-fractional Black–Scholes European option pricing problem arising in financial market, *Applied Mathematical Sciences* 7 (69) (2013) 3445–3456.
- [27] H. Mesgarani, A. Beiranvand, Y. E. Aghdam, The impact of the Chebyshev collocation method on solutions of the time-fractional Black–Scholes, *Mathematical Sciences* 15 (2) (2021) 137–143.
- [28] X. An, F. Liu, M. Zheng, V. V. Anh, I. W. Turner, A space-time spectral method for time-fractional Black-Scholes equation, *Applied Numerical Mathematics* 165 (2021) 152–166.
- [29] T. Akram, M. Abbas, K. M. Abualnaja, A. Iqbal, A. Majeed, An efficient numerical technique based on the extended cubic B-spline functions for solving time fractional Black–Scholes model, *Engineering with Computers* (2021) 1–12.



- [30] V. Gupta, M. K. Kadalbajoo, Qualitative analysis and numerical solution of burgers' equation via b-spline collocation with implicit euler method on piecewise uniform mesh, *Journal of Numerical Mathematics* 24 (2) (2016) 73–94.
- [31] M. K. Kadalbajoo, V. Gupta, A parameter uniform b-spline collocation method for solving singularly perturbed turning point problem having twin boundary layers, *International Journal of Computer Mathematics* 87 (14) (2010) 3218–3235.
- [32] M. K. Kadalbajoo, V. Gupta, Numerical solution of singularly perturbed convection–diffusion problem using parameter uniform b-spline collocation method, *Journal of Mathematical Analysis and Applications* 355 (1) (2009) 439–452.
- [33] M. K. Kadalbajoo, V. Gupta, A. Awasthi, A uniformly convergent b-spline collocation method on a nonuniform mesh for singularly perturbed one-dimensional time-dependent linear convection–diffusion problem, *Journal of Computational and Applied Mathematics* 220 (1) (2008) 271–289.
- [34] S. Pruess, Alternatives to the exponential spline in tension, *Mathematics of Computation* 33 (148) (1979) 1273–1281.
- [35] S. Pruess, Properties of splines in tension, *Journal of Approximation Theory* 17 (1) (1976) 86–96.
- [36] C. De Boor, C. De Boor, A practical guide to splines, Vol. 27, Springer-Verlag, New York, 1978.
- [37] B. J. McCartin, Theory of exponential splines, *Journal of Approximation Theory* 66 (1) (1991) 1–23.
- [38] S. C. S. Rao, M. Kumar, Exponential b-spline collocation method for self-adjoint singularly perturbed boundary value problems, *Applied Numerical Mathematics* 58 (10) (2008) 1572–1581.
- [39] X. Zhu, Y. Nie, Z. Yuan, J. Wang, Z. Yang, An exponential B-spline collocation method for the fractional sub-diffusion equation, *Advances in Difference Equations* 2017 (1) (2017) 1–17.
- [40] A. S. V. Ravi Kanth, N. Garg, A computational procedure and analysis for multi-term time-fractional burgers-type equation, *Mathematical Methods in the Applied Sciences* n/a (n/a) (2022). doi:<https://doi.org/10.1002/mma.8299>.
- [41] A. S. V. Ravi Kanth, N. Garg, An unconditionally stable algorithm for multiterm time fractional advection–diffusion equation with variable coefficients and convergence analysis, *Numerical Methods for Partial Differential Equations* 37 (3) (2021) 1928–1945.

- [42] I. Podlubny, Fractional differential equations: an introduction to fractional derivatives, fractional differential equations, to methods of their solution and some of their applications, Elsevier, 1998.
- [43] C. Li, F. Zeng, Numerical methods for fractional calculus, Chapman and Hall/CRC, 2019.
- [44] S. T. Mohyud Din, T. Akram, M. Abbas, A. I. Ismail, N. H. Ali, A fully implicit finite difference scheme based on extended cubic B-splines for time fractional advection–diffusion equation, *Advances in Difference Equations* 2018 (1) (2018) 1–17.
- [45] H. M. Zhang, F. W. Liu, I. Turner, S. Chen, The numerical simulation of the tempered fractional Black–Scholes equation for European double barrier option, *Applied Mathematical Modelling* 40 (11-12) (2016) 5819–5834.